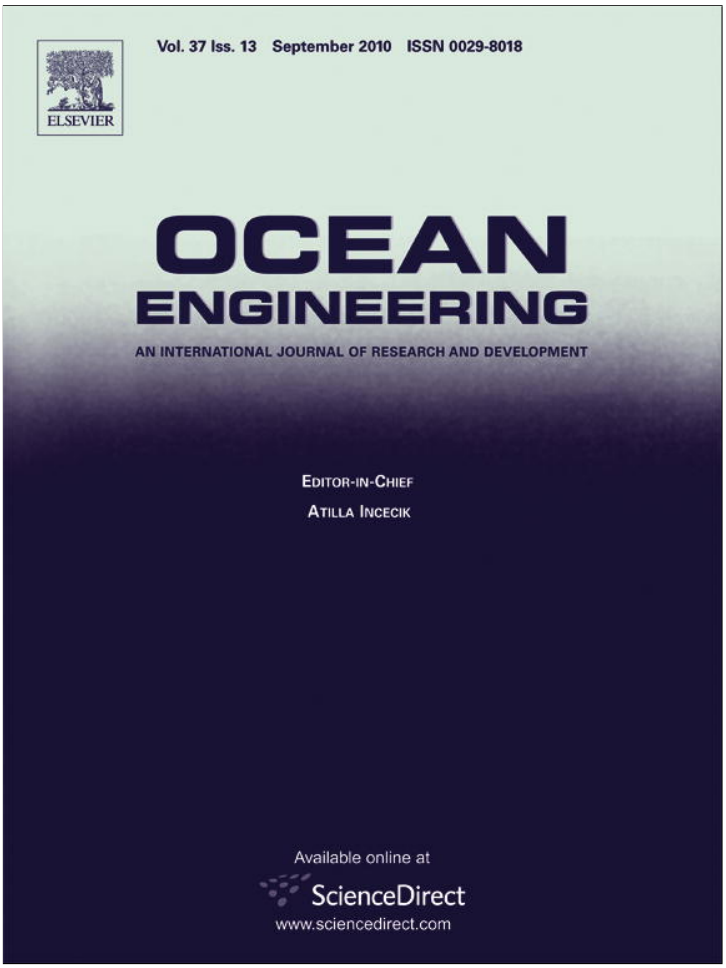

Ocean Engineering 37 (2010) 1193–1220

Contents lists available at ScienceDirect

Ocean Engineering

journal homepage: www.elsevier.com/locate/oceaneng

Nonlinear adaptive control of an underwater towed vehicle

Francisco Curado Teixeira [a,*], António Pedro Aguiar [b], António Pascoal [b]

[a] Center for Environmental and Marine Studies and Department of GeoSciences, University of Aveiro, Campus Universitário de Santiago, 3810-193 Aveiro, Portugal
[b] Institute for Systems and Robotics and Department of Electrical Engineering, Instituto Superior Técnico, Av. Rovisco Pais 1, 1049-001 Lisboa, Portugal

ARTICLE INFO

Article history:
Received 10 October 2009
Accepted 30 May 2010
Available online 19 June 2010

Keywords:
Nonlinear control
Adaptive control
Lyapunov methods
Trajectory tracking
Underwater
Towed vehicle

ABSTRACT

This paper addresses the problem of simultaneous depth tracking and attitude control of an underwater towed vehicle. The system proposed uses a two-stage towing arrangement that includes a long primary cable, a gravitic depressor, and a secondary cable. The towfish motion induced by wave driven disturbances in both the vertical and horizontal planes is described using an empirical model of the depressor motion and a spring-damper model of the secondary cable. A nonlinear, Lyapunov-based, adaptive output feedback control law is designed and shown to regulate pitch, yaw, and depth tracking errors to zero. The controller is designed to operate in the presence of plant parameter uncertainty. When subjected to bounded external disturbances, the tracking errors converge to a neighbourhood of the origin that can be made arbitrarily small. In the implementation proposed, a nonlinear observer is used to estimate the linear velocities used by the controller thus dispensing with the need for costly sensor suites. The results obtained with computer simulations show that the controlled system exhibits good performance about different operating conditions when subjected to sea-wave driven disturbances and in the presence of sensor noise. The system holds promise for application in oceanographic missions that require depth tracking or bottom-following combined with precise vehicle attitude control.

1. Introduction

Underwater towed vehicles (tow-fishes) have found widespread utilization in the acquisition of oceanographic data. In many missions of interest, the vehicles are passive and their motion is controlled via a cable connecting them to a support ship. However, increasingly demanding missions scenarios require far better control of the tow-fish underwater, including simultaneous depth and precise attitude control under environmental disturbances. For this reason, there is currently increasing interest in the development of controlled underwater towed vehicles.

In terms of depth control, two related problems may be posed. The first arises in the scope of physical and biological oceanographic missions and consists of tracking a depth profile which is independent of the topography of the sea-floor. The second problem arises in the context of bottom-following missions and consists of maintaining a desired altitude above the sea-bottom; the latter is a common requirement, in particular for marine geophysical data acquisition. Simultaneous depth and attitude control is normally required since in some applications the attitude of the towfish may affect significantly the quality of the data acquired.

1.1. Applications and main motivation

Applications of underwater towed vehicles in physical oceanography include the deployment of current profilers for sampling of small-scale ocean turbulence; see e.g. Gargett (1994) and Spain and Fortin (1994). In this type of application, stabilization of the towfish in pitch and roll is necessary to guarantee good data accuracy; yaw disturbances can be tolerated provided that they do not induce significant pitch and roll motions that would violate the tilt specifications imposed by the acoustic methods (Schuch et al., 2005).

In marine geophysics, common applications include the use of side-scan-sonar systems, and marine vector magnetometers and gravimeters; see for example Parker (1997), Zumberge et al. (1997), and Tivey et al. (1998). For sonar imaging, pitch and yaw rates may have a greater impact on image distortion than pitch and yaw angles since distortion depends on the change of attitude during the short time interval in which the image is recorded. The problems associated with side-scan sonar acquisition are analysed by Preston (1992), Preston and Shupe (1993), and Preston and Poeckert (1993). It is shown in these references that even small errors in yaw can distort severely the sonar images and

* Corresponding author. Tel.: +351 234370357; fax: +351 234370605.
E-mail addresses: fcurado@ua.pt, fjcurado@gmail.com (F. Curado Teixeira), pedro@isr.ist.utl.pt (A. Pedro Aguiar), antonio@isr.ist.utl.pt (A. Pascoal).

0029-8018/$ - see front matter © 2010 Elsevier Ltd. All rights reserved.
doi:10.1016/j.oceaneng.2010.05.010

make the detection of small objects impossible. Although post-processing techniques can be applied to remove some of the deleterious effects, their effectiveness is limited by the degree of distortion imparted on the acoustic imagery by towfish motion. An analysis of the combined effects of yaw and pitch motions and the results of application of real time and offline correction methods to multibeam sonar data is presented by Cappell et al. (1993). The study demonstrates the limitations of the methods when applied to very wide swath multibeam data.

The problem that we address was primarily motivated by the need to acquire vectorial measurements of the geomagnetic field and geomagnetic gradients close to the sea-bottom using marine vector magnetometers. Marine magnetic surveying is a very important tool in geophysical exploration. It is routinely applied to oil exploration to locate oil traps within sediments or topographic features of the basement that can influence the overlying sedimentary cover. Magnetometry is also an important tool in pipeline detection and tracking, mine hunting, and marine archaeology, among others. The latter applications normally involve small magnitude anomalies and require good signal-to-noise ratio.

Marine magnetometers are typically towed by research vessels as a form of mitigating the effects of noise induced by the ship. Another reason to deploy the magnetometers in a towed platform is the ability to perform near-bottom surveys in deep waters. This is justified because the amplitude of magnetic signals generated by shallow geological bodies is sharply attenuated with increasing distance to the sources of the anomalies. For this reason, it is convenient for many applications to execute the survey as close to the sea-bottom as possible, employing a vehicle that can follow the terrain topography. More recently this type of surveys has started to be executed by ROVs and AUVs; see Tivey et al. (1998) and Tivey and Johnson (2002). However, due mainly to the noise introduced by the vehicle thrusters this method incurs a significant reduction of the signal-to-noise ratio. Hence, towing the magnetometer by a ship or an AUV is still the preferred method to locate the sensors away from the main sources of magnetic noise.

It is well known that the accuracy of measurements of the geomagnetic field vector is largely dictated by orientation errors due to the large differences of the components of the Earth's background field. Since magnetic gradient measurements are much less affected by sensor misalignments and orientation errors, in many applications it is convenient to measure the geomagnetic gradient or one of its components. In marine applications it is normally preferable to measure the vertical gradient since it does not impose any restriction on the heading of the sensors and is considerably more affordable than measuring the three orthogonal components. However, to measure the vertical gradient with high accuracy it is necessary to use a platform stabilized in pitch and roll.

Motivated by the above problems, this paper addresses the simultaneous problem of depth and attitude control of an underwater towed vehicle.

The organization of the paper is as follows: in the remainder of this section we present prior and related work and summarize the proposed approach as well as our main contributions. Section 2 introduces the main physical characteristics of the system under study and the desired performance specifications, as well as the models of the towing arrangement and external disturbances. Section 3 describes the dynamical model of the vehicle and formulates the problem of depth tracking and attitude control in the presence of external disturbances and parametric model uncertainty. In Section 4, a solution to this problem is proposed in terms of a nonlinear adaptive control law. Section 5 presents a nonlinear observer for estimation of the heave velocity used by the controller, assuming that no direct measurements of surge, sway, and heave velocities of the vehicle are available for feedback. Section 6 evaluates the performance of the control algorithms developed using computer simulations. Finally, Section 7 contains some concluding remarks and proposes some guidelines for further research.

1.2. Prior and related work

1.2.1. Towing arrangements

Towing systems play a crucial role in marine operations. For this reason, the last decades have witnessed considerable research work on the dynamics of towing cables and towed vehicles. See for example Abkowitz (1969) for an introductory exposition of this topic.

Towing systems can be classified into two main types: single-part and two-part. Distinct models are needed to capture their dynamic behaviour. In the first type of arrangement, the dominant motion of the towing system is that due to the coupling between the ship and the towing cable. For this reason, considerable effort has been devoted to the study of towing cable dynamics. See e.g. Kato (1987), Kato et al. (1986), Joannides and Le Gland (1993), Yokobiki (2000), Yamaguchi et al. (2000), Buckham et al. (2003), Toda (2005) and the references therein. The need to determine accurately the position of a towed vehicle at the end of a long towing cable constitutes another motivation to model the behaviour of towing cables. The latter subject is addressed in Perrault et al. (1997) and Damy et al. (1994). Modelling is restricted to the vertical plane. Damy et al. (1994) propose a model for the towing cable to transform position measurements of the towing vessel obtained by GPS into estimates of position and velocity of the towed vehicle. Calkins (1999) studies the lateral motion of a towed body in response to ship manoeuvres. Most of these studies adopt the *lumped mass* approach to model long towing cables.

Although characterized by greater complexity of deployment, two-part towing arrangements (see Fig. 1) achieve superior performance in terms of rejection of the disturbances transmitted to the towing system. A study of this type of system is presented in Preston (1992), where the effects of wave-driven motions of the towing vessel on a sonar platform are discussed. The results of sea-trials demonstrate that a two-stage towing arrangement can significantly attenuate towfish attitude disturbances due to the surface ship motion. The performance of this type of towing arrangement is analysed in more recent research work that addresses the problem of towfish control; see Wu and Chwang (2000,2001a, b). In particular, Wu and Chwang (2001b) propose a numerical model to investigate the hydrodynamic behaviour of an underwater vehicle in a two-part

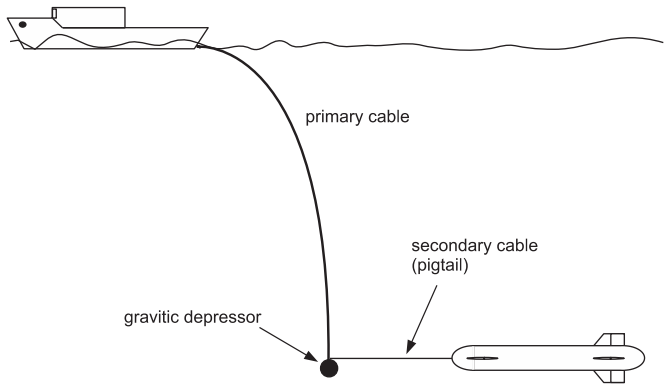

Fig. 1. Two-part towing arrangement.

towing arrangement where the depressor is equipped with active horizontal and vertical control surfaces.

1.2.2. Control problem formulations

In the literature, two main approaches can be found to the problem of towfish control: one addresses the problem only in the vertical plane (including depth and pitch); the second addresses control in both the vertical and horizontal planes (including control of depth, pitch, yaw, and lateral position). In general, the problem of motion in roll is neglected. Alternatively, roll stability is ensured through a combination of hydrodynamic damping and placement of the center of buoyancy of the vehicle (Wu et al., 2005). For several marine applications, controlling the depth and the attitude of the vehicle in the vertical plane is sufficient. This approach is adopted by several authors; see e.g. Yamaguchi et al. (2000), Yokobiki (2000), and Wu et al. (2005). A distinct approach to pitch stabilization is adopted by Woolsey and Gargett (2002) who propose a towfish equipped with a servo-actuated mass that can trim the vehicle's center of gravity. This solution is practical at very low towing speeds, when the actuated control surfaces become ineffective.

The problem of simultaneous control in vertical and horizontal planes is addressed in Wu and Chwang (2001b) but the controller proposed is not designed to react to perturbations in the horizontal plane. Furthermore, the vertical control surfaces are used only to direct the vehicle along a desired path. As a consequence, the performance achieved in yaw assessed in simulation is less than satisfactory. In Kato (1991) the problem of controlling the attitude, altitude, and lateral position of an underwater vehicle towed with a single cable is addressed using a decoupled model of vertical and horizontal motions. Encouraging results are obtained with the controlled system simulated under the influence of disturbances caused by sea waves and tidal currents. A fully 3D-control of a hybrid autonomous underwater vehicle (AUV)/towfish system is addressed in Choi et al. (2005). Recent studies include other non-conventional approaches such as towing by an AUV or an autonomous surface vehicle (ASV); see Buckham et al. (2003) and Lambert et al. (2003). In some cases, the towed vehicle is equipped with thrusters to enhance the control capabilities of the system; see Wu et al. (2005).

1.2.3. Controller design and implementation methods

In terms of controller design, the methods normally employed for towed vehicle control assume that the towfish is operated close to some equilibrium point and rely on the linearisation of the vehicle dynamics about that point. In most of the work cited in the literature, the authors resort to PID control. Campa et al. (1996) propose a model-based controller that addresses robustness issues such as uncertainties in the determination of system parameters and errors introduced by linearisation of the system dynamics in a H_∞ framework. This work reports the same problem mentioned in Perrault et al. (1997): there is a tradeoff between good altitude control and pitch control. The problem of depth control for a direct tow is addressed by Nasuno et al. (2008) resorting to linear matrix inequalities (LMIs). The controller derived is suitable for different equilibrium conditions under the assumption of small heave forces and small cable vibration disturbances.

1.2.4. Experiment based modelling

Since in the model proposed in this study the motion of the towfish is derived from the motion of the gravitic depressor, we emphasize the importance of using a realistic simulation of depressor motion. To assess the consistency of the approach presented in this work we studied other models of depressor motion described in the literature and analysed how closely our model reproduces their theoretical and experimental results. Particularly relevant for the present work are the results reported by Preston (1989), Preston (1992) and Preston and Shupe (1993), obtained in trials at sea with different types of towing arrangements and towed vehicles. The experimental results obtained by Wu and Chwang (2001a) with a scaled model and by Hopkin et al. (1993) with full-scale experiments in a towing tank constitute also important references in the present context. These results will be discussed in Section 2.

1.3. Proposed approach and main contributions of the work

One of the main drawbacks of the aforementioned controller design formulations stems from the fact that they rely on linearisation of the system dynamics in the neighbourhood of a few operating points. This approach has limited applicability to the solution of the problem at hand since the motion of the underwater towed vehicle can be largely influenced by external disturbances resulting in large excursions over a wide range of operating conditions. As a contribution to overcoming well known limitations, in the present work the problem of towfish control is addressed in the scope of nonlinear control theory. The study that we perform resorts to nonlinear model-based design and employs stability analysis tools to handle the nonlinearities of the system in a large operation range. This approach was dictated mainly by the requirement that the controller should yield good performance when the vehicle undergoes motions about different equilibrium conditions and exhibit robustness against vehicle parameter uncertainty. The equilibrium conditions are determined by, among other factors, the pigtail length and the towing speed. The vehicle dynamic model adopted builds on previous work in Teixeira et al. (2006). However, in the present version we tackle the problem of controlling the vehicle's depth and attitude in both the vertical and horizontal plane, not just in the vertical plane.

The key contributions of the present paper are twofold:

1. An adaptive control structure is proposed that exhibits good performance about different equilibrium conditions and is robust against vehicle parameter uncertainty. The nonlinear control law derived is proven to stabilize the system in the presence of bounded external disturbances and unmodelled dynamics.
2. Controller design assumes explicitly that no direct measurements are available of surge, sway, and heave speeds. In contrast with previous work in Teixeira et al. (2006), a nonlinear observer is used to estimate these variables.

2. System characteristics and modelling

2.1. System characteristics

In the present study the towfish specification and key towfish hydrodynamic parameters are derived from the configuration proposed in Schuch (2004) and Schuch et al. (2005). Additional parameters are based on those commonly used in the design of underwater vehicles; see e.g. Pascoal et al. (1997) and Silvestre and Pascoal (1997). For safety reasons, the towfish has slightly positive buoyancy.

2.1.1. Towing system

The towing system that we consider consists of a two-part towing arrangement as illustrated in Fig. 1. The nose of the towfish is connected via a small umbilical (the pigtail section) to a

gravitic depressor, which is in turn connected to and towed by a support ship using a long tow line (the primary cable).

2.1.2. Vehicle characteristics

The proposed vehicle is equipped with a bow plane, a stern plane, and a rudder. The bow and stern control planes are equidistant from the vehicle's center of mass; see Fig. 2. The sensor suite proposed includes an attitude and heading unit (AHU), a depth sensor, and optionally a sonar altimeter. The towfish has a slightly positive buoyancy and the metacentric height is such that the vehicle is naturally stabilized in roll.

The towing arrangement proposed includes a communications' cable between the towed vehicle and the towing vessel for transmission of control signals and data. Although in some mission scenarios the system proposed may dispense with the need for a cabled communication link between the towfish and the support vessel, the classical cabling solution is recommended to allow for real-time monitoring of system operation and on-board data recording.

2.2. Performance specifications

The system's performance specifications are dictated by the requirements imposed by different mission scenarios that include geomagnetic surveying, deployment of current profilers, and sonar imaging. The specification for the maximum depth error is dictated by the desired bound on the variations of the magnetic readings caused by variations of the surveying altitude. The errors so originated are very difficult to correct in post-processing due to the nonlinear character of potential fields' scaling; see e.g. Blakely (1995). Based on the requirements of some typical scenarios of operation we require the towed vehicle to regulate the depth error to zero ± 0.30 m. This specification is justified in Appendix A. The tilt specifications for the proposed towed vehicle are dictated by the requirements of the acoustic methods used in sonar imaging applications and physical oceanography, cf. Preston (1992) and Schuch et al. (2005). The controller is required to regulate the pitch angle and the yaw error to zero ± 1 deg while the towing system and the vehicle are designed to passively stabilize the attitude in roll. The towing speed is expected to vary between 3 and 8 knts, depending on the type of oceanographic mission.

2.3. Analysis of previous towing models

The sheathed model proposed by Chapman (1982), which approximates the behaviour of a Bowden cable, decomposes motions of the top of the main cable into two components—parallel and transverse to the upper cable segment. That model is applied to determine the motion of 100 m of faired cable where the cable top (at the vessel towing point) is subjected to periodic oscillations. The simulation results show that after a certain time the fish adopts a cyclic motion; the locus of the bottom end of the cable approximates an ellipse with a large eccentricity. The ratio of the ellipse's minor axis to the ship motion amplitude is determined for different periods of oscillation. The work considers a neutrally stable body with isotropic drag that behaves like a sphere with constant drag coefficient; this corresponds to the configuration of our gravitic depressor. According to the authors, the Bowden cable behaviour provides a very good approximation to the response of a towed weight to random disturbances.

Hubbard (1993) shows that the most effective form of mitigating disturbance propagation through the towing cables consists in forcing the lower towline axis (either in a single tow or in a two-part tow) to be coaxial with the towfish axis of symmetry. To implement this procedure, an approximately neutrally buoyant towfish is required. With this method, the axial motion of the towline produces dominantly fore-aft accelerations of the towed vehicle.

The model of the wave-induced disturbances that we adopt takes in consideration the results mentioned below.

Preston and Shupe (1993) show that heave of the towing point in different ships is the variable that is least dependent on the encounter angle while sway is approximately equal in head and following seas and surge is the most dependent on ship configuration. Wu and Chwang (2000) conclude that the two-part tow method has practically no influence on the surge and sway behaviour of the towfish. They show that the heaving ratio between the towed vehicle and the depressor depends on the encountering frequency of the towing ship and the length of the secondary cable. The ratio decreases for increasing encountering frequency and increasing secondary cable length. Hence, Wu and Chwang (2000) suggest that in order to improve the stability of a towed vehicle during survey operations it is advisable to select a sufficiently long secondary cable and to keep the towing vessel in a convenient wave aspect such as head sea towing. These conclusions are supported by the experimental results obtained by Hopkin et al. (1993) in tow tank experiments at full-scale. These results show also that the heave amplitude ratio increases with increasing towing speed. In this respect we notice an apparent contradiction in the conclusions drawn by Wu and Chwang (2001a) suggesting that the towfish/depressor heave ratio is smaller for lower towing speeds. Actually, a closer analysis of the experimental results presented in Wu and Chwang (2001a) shows that for towing speeds larger than 1.5 m/s the heaving ratio effectively increases with increasing towing speed.

2.4. Notation

In what follows, $\{I\}$ represents an inertial coordinate frame and $\{B\}$ denotes a body-fixed frame that moves with the vehicle. The referential associated with the secondary cable that is defined in a forthcoming section is denoted $\{C\}$. Following standard notation (Fossen, 2002), the vector $\eta := [x,y,z,\phi,\theta,\psi]$ represents the position and orientation of the vehicle expressed in $\{I\}$ and $\nu := [u,v,w,p,q,r]$ denotes the linear and angular components of the velocity of the vehicle expressed in $\{B\}$. When convenient, we also

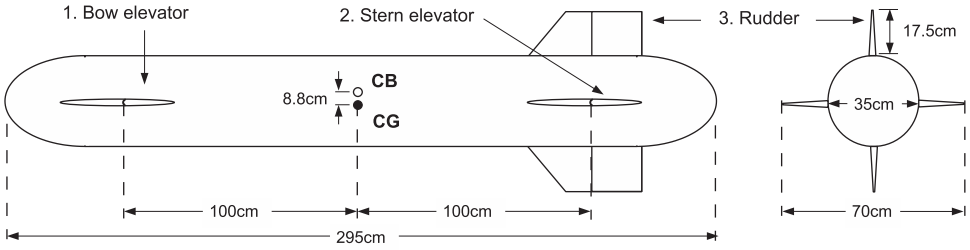

Fig. 2. Physical dimensions of the towfish. The fins and control surfaces are grouped in pairs and numbered according to this figure.

use vectors $\eta_1 \coloneqq [x,y,z]$ to represent the position of the origin of $\{B\}$ expressed in $\{I\}$ and $\eta_2 \coloneqq [\phi,\theta,\psi]$ to represent the Euler angles. The velocity vector is also usually decomposed into the linear velocities represented by $v_1 \coloneqq [u,v,w]$ and the angular velocities represented by $v_2 \coloneqq [p,q,r]$.

Whenever necessary, to simplify the notation the following abbreviations are used: $s\cdot \coloneqq \sin(\cdot)$, $c\cdot \coloneqq \cos(\cdot)$, and $t\cdot \coloneqq \tan(\cdot)$. The symbol $\times$ is used to denote vector *cross product*. The matrix *trace* operator is denoted by $\mathbf{tr}(\cdot)$. A list of the symbols used in the paper is presented in Tables 1–4. Refer also to Tables 5 and 6 for a list of other variables used in simulations.

2.5. 6DOF equations of motion

The simulation of the vehicle dynamics is implemented using the three-dimensional 6*DOF* equations of motion represented in compact form by (see e.g. Fossen, 2002)

$$M\dot{v}+C(v)v+D(v)v+g(\eta)=\tau+\tau_e,$$

$$\dot{\eta}=J(\eta_2)v, \tag{1}$$

Table 1
System model notation.

$\{B\}$	Body-fixed reference frame
$\{C\}$	Secondary cable reference frame
$\{I\}$	Inertial reference frame
AR	Aspect ratio of a control surfaces
$\overline{b}$	Damping coefficient of pigtail
$\overline{B}$	Buoyancy of towfish
$C(\cdot)$	Coriolis and centripetal matrix
$C_{L\alpha\beta}$	Approximate gradient of the hull lift coefficient as a function of the angles α and β
$C_{L\alpha}$	Approximate gradient of the fins lift coefficient as a function of the angles α or β
$C_{M\alpha\beta}$	Approximate gradient of the hull pitch damping coefficient as a function of the angles α and β
$C_{N\alpha\beta}$	Approximate gradient of the hull yaw damping coefficient as a function of the angles α and β
$C_A(\cdot)$	Hydrodynamic Coriolis and centripetal matrix
$C_{RB}(\cdot)$	Rigid-body Coriolis and centripetal matrix
$C_K(\cdot)$, $C_M(\cdot)$, $C_N(\cdot)$	Hydrodynamic damping coefficients of the hull moments associated with roll, pitch, and yaw
$C_x(\cdot)$, $C_y(\cdot)$, $C_z(\cdot)$	Hydrodynamic damping coefficients of the hull forces in surge, sway, and heave
$D(\cdot)$	Hydrodynamic damping matrix
E_c	Elastic modulus of pigtail
$f_v(\cdot)$	Dynamic pressure function
$g(\cdot)$	Vector of restoring forces and moments expressed in the body-fixed frame
$J(\cdot)$	Rotation matrix transforming the position and orientation vector from $\{B\}$ to $\{I\}$
$J_1(\cdot)$	Rotation matrix transforming the position vector from $\{B\}$ to $\{I\}$
$J_2(\cdot)$	Rotation matrix transforming the orientation vector from $\{B\}$ to $\{I\}$
$\overline{k}$	Spring constant of pigtail
L_B	Length of the body of the towfish
L_C	Length of the secondary cable (pigtail)
$\overline{m}$	Mass of the vehicle
M	System inertia matrix
M_A	Hydrodynamic inertia matrix
M_{RB}	Rigid-body inertia matrix
p_d	Position of the depressor expressed in $\{I\}$
r_x, r_y, r_z	Normalized 3D components of the depressor excursion expressed in $\{I\}$
R_B^I	Rotation matrix equal to $J_1(\eta_2)$
R_C^I	Rotation matrix from $\{C\}$ to $\{I\}$
S_s	Planform area of the rudder and horizontal planes, tip to tip
$\overline{W}$	Dry weight of towfish
x_F^i	x-Coordinate of the hydrodynamic center of the ith fin expressed in the body-fixed frame

Table 2
Controller and observer notation.

a_1, a_2, a_3	True values of system parameters used in matrices Γ_1,Γ_2, and Γ_3
$\hat{a}_1$,$\hat{a}_2$,$\hat{a}_3$	Estimated values of a_1, a_2, and a_3
A	Matrix defined from system parameters a_1, a_2, a_3
$\hat{A}$	Estimated value of matrix A
d	Vector representing the effect of external forces and moments in system dynamics, expressed in $\{B\}$
$\overline{e}$	Tracking error vector
$\overline{e}_z$, $\overline{e}_\theta$, $\overline{e}_\psi$	Components of the tracking error vector in depth, pitch, and yaw, respectively
$f_o(\cdot)$	State independent observer component
$f_w(\cdot)$	Vehicle hydrodynamic forces associated with heave
$f_\theta(\cdot)$	Vehicle hydrodynamic forces associated with pitch
$f_\psi(\cdot)$	Vehicle hydrodynamic forces associated with yaw
F_θ	Observer nonlinear dynamic matrix
$g_o(\cdot)$	State dependent observer component
$g_w(\cdot)$	Vehicle restoring force associated with heave
$g_\theta(\cdot)$	Vehicle restoring moment associated with pitch
$g_\psi(\cdot)$	Vehicle restoring moment associated with yaw
h	Measurement coupling matrix of the observer
H	Observer linear dynamic matrix
$K_o(\cdot)$	Nonlinear gain of the observer
n_z	Depth measurement noise
q	Pitch rate
r	Yaw rate
$\overline{u}$	Control variable
u	Surge velocity
v	Sway velocity
w	Heave velocity
$\hat{w}$	Heave velocity estimated by the observer
x_o	Observer state
$\hat{x}_o$	Observer estimated state
$\tilde{x}_o$	Observer error
y_o	Measurements used by the observer
$\hat{y}_o$	Observer estimated measurements
z	Depth of the vehicle
z_d	Desired depth
$X_1=[z,\theta,\psi]'$	Pose of the vehicle expressed in $\{I\}$ in the simplified motion model
$X_2=[w,q,r]$	Velocity of the vehicle relative to $\{B\}$ in the simplified motion model

Table 3
System model notation (Greek).

η	Position and orientation vector expressed in $\{I\}$
η_1	Position of the origin of $\{B\}$ expressed in $\{I\}$
η_2	Vector of Euler angles
ε_s	Span efficiency factor of control surfaces
ζ	Pigtail damping ratio
v	Velocity vector expressed in the body-fixed frame
v_1	Vector of linear velocities of the vehicle expressed in $\{B\}$
v_2	Vector of angular velocity of the vehicle expressed in $\{B\}$
ρ	Density of water
τ_{e_f}	Vector of external forces applied to the towfish expressed in $\{B\}$
τ_{e_m}	Vector of external moments applied to the towfish expressed in $\{B\}$
τ	Vector of forces and moments generated by the control surfaces expressed in frame $\{B\}$
τ_u,τ_v,τ_w,τ_ϕ,τ_θ,τ_ψ	Components of τ
ϕ_x, ϕ_y, ϕ_z	Phase delays of each of the 3D components of the periodic motion of the depressor
ω_0	Modal frequency of the JONSWAP wave spectrum
ω_e	Frequency of encounter
ΔL	Distance between the depressor and the towing point in the towfish
Δv	Difference between the velocity of the depressor and the towfish velocity at the tow-point, expressed in $\{I\}$
Δy	y-Axis distance between the depressor and the towfish tow-point in referential $\{I\}$
Δz	z-Axis distance between the depressor and the towfish tow-point in referential $\{I\}$

Table 4
Controller and observer notation (Greek).

α	Angle of attack
β	Angle of side-slip
δ	Vector of deflection angles of control surfaces
δ_b, δ_s, δ_r	Deflection angles of bow, stern and rudder control surfaces, respectively
δ_o	Heave force used by the observer
θ	Pitch angle of the vehicle
σ_1, σ_2, σ_3	Functions of measured variables used in the linear parametric model
σ_{c1}, σ_{c2}, σ_{c3}	Additional functions corresponding to the vertical/horizontal coupling terms
τ_o	Estimation error of the nonlinear component of observer
ψ	Yaw angle of the vehicle
ψ_d	Desired yaw
Γ_1, Γ_2, and Γ_3	Matrices of system parameters in the linearly parametrized formulation
Γ_{c1}, Γ_{c2}, and Γ_{c3}	Additional matrices corresponding to the vertical/horizontal coupling terms
$\hat{\Gamma}_1$, $\hat{\Gamma}_2$, and $\hat{\Gamma}_3$	Estimated values of Γ_1,Γ_2, and Γ_3
Ω_c	Vector representing the coupling components of the system dynamics due to motion in roll

Table 5
Values of system parameters used in the simulations.

Parameter	Symbol	Value	Units
Added mass and inertia	$X_{\dot{u}}$	−8.7849	kg
	$X_{\dot{w}}$	0	kg
	$Y_{\dot{v}}$	−18.64	kg
	$X_{\dot{q}}$	0	kg m
	$Y_{\dot{p}}$	0	kg m
	$Y_{\dot{r}}$	0	kg m
	$Z_{\dot{q}}$	−1.5	kg m
	$Z_{\dot{u}}$	−1.1	kg
	$Z_{\dot{w}}$	−18.64	kg
	$K_{\dot{v}}$	0	kg m
	$M_{\dot{u}}$	−2.0	kg m
	$M_{\dot{w}}$	−1.6	kg m
	$N_{\dot{v}}$	−1.6	kg m
	$K_{\dot{p}}$	−60	kg m^2
	$K_{\dot{r}}$	0	kg m^2
	$M_{\dot{q}}$	−260.55	kg m^2
	$N_{\dot{p}}$	−60	kg m^2
	$N_{\dot{r}}$	−260.55	kg m^2
Moments and products of inertia	I_{xx}	17.4	kg m^2
	I_{yy}	174.49	kg m^2
	I_{zz}	174.49	kg m^2
	I_{xz}	1.74	kg m^2
Hydrodyn. damping	$K_{\|p\|p}$	−125	kg m^2
	$M_{\|q\|q}$	−500	kg m^2
	$N_{\|r\|r}$	−500	kg m^2
	$Z_{\|q\|q}$	−10	kg m^2
	$Y_{\|r\|r}$	10	kg m^2
Mass of the towfish	$\overline{m}$	113.5	kg
Towfish dry weight	$\overline{W}$	1112	N
Volume of hull	$\overline{V}$	1	m^3
Buoyancy force	$\overline{B}$	1167.6	N
Length of the body	L_b	2.75	m
Center of gravity (CG)	(x_G,y_G,z_G)	(0,0,0)	m
Center of buoyancy (CB)	(x_B,y_B,z_B)	(0,0,−0.08)	m
Gradient of body lift coeff.	$C_{L\alpha\beta}$	0.3508	–
Gradient of body pitch coeff.	$C_{M\alpha\beta}$	0.1308	–
Length of pigtail	L_c	100 or 50	m
Elastic modulus of pigtail	E_c	5E+4	N
Pigtail damping ratio	ζ	1	–
Gradient of fin lift coeff.	$C_{L\alpha}$	5.24	–
Planform area of fins	S_s	1.36	m^2
Fin aspect ratio	AR	6.8	–
Span efficiency factor	ε_s	0.97	–
Coordinates of fin num. 1	(x_f^1,y_f^1,z_f^1)	(1,0,0)	m
Density of water	ρ	1000	kg m^{-3}

Table 6
General simulations' parameters.

Type of parameter	Symbol	Value	Units
Initial conditions			
Bottom following	X_1	[0, 0, 15]′	m
Synthetic profile	X_1	[0, 0, 22.5]′	m
Constant depth	X_1	[0, 0, 30]′	m
Initial velocities	$[u,v,w]'$	[0,0,0]′	m/s
Initial angular rates	$[p,q,r]'$	[0,0,0]′	rad/s
Velocity of ocean current	V_w	[−0.5,0.25,0]′	m/s
Velocity bounds	b_w	1	m/s
	b_v	0.2	m/s
	b_p	0.5	rad/s
Controller gains	K_a	diag(10,5,50)	
	K_b	diag(5,10,10)	
	m	1.0E−8	
	n	1.5E+6	
Observer gains (minima)	$[k_1,k_2]'$	[10,10]′	
Measurement noise std. dev.	σ_z	0.1	m
	σ_θ	0.1	deg
	σ_ψ	1	deg
	σ_q	0.5	deg/s
	σ_r	0.5	deg/s
Parameters of wave-driven disturbances			
	r_x	0.1	
	r_y	0.01	
	r_z	0.89	
	ϕ_x	$\pi/4$	rad
	ϕ_y	$\pi/2$	rad
	ϕ_z	0	rad
JONSWAP parameters			
Significant wave height	H_s	1.5	m
Modal frequency	ω_o	0.4	rad/s
Max. frequency	ω_{max}	1.5	rad/s
Num. spectral components	N	100	

where M is the system inertia matrix, $C(v)$ is the Coriolis and centripetal matrix, $D(v)$ is hydrodynamic damping matrix, and $J(\eta)$ represents the transformation matrix from the body-fixed frame $\{B\}$ to the inertial coordinate frame $\{I\}$. The forces and moments due to actuation of the control surfaces are represented by τ. The vector τ_e represents the external forces and moments acting on the system expressed in the body-fixed referential, including the effects of the towing forces and moments, and the external disturbances. The expanded model is presented in Appendix B.

2.6. Towing system and wave models

In the present study, the towing system is simulated in a simplified manner by assuming that the perturbations induced by sea-waves are transmitted to the depressor without attenuation. Thus, the motion of the depressor corresponds to the motion of the towing point at the towing ship. The cable section connecting the depressor to the towfish is modelled as a spring-damper system similar to the one proposed by Schuch (2004) where the spring constant is a function of cable characteristics while damping is imposed by the towfish. Although this is a simplified model it can be interpreted as a "worst case" scenario. In this towing arrangement, the length of the pigtail can be used as a design parameter to filter the effects of the disturbances transmitted to the depressor through the primary cable.

2.6.1. Modelling cable tension forces

Consider the two-part towing system with a secondary towing cable connecting directly the depressor weight to the nose of the towfish as illustrated in Fig. 3. A cable-fixed reference frame $\{C\}$ is defined having its x-axis collinear with the secondary cable and pointing in the direction of the depressor. The origin of $\{C\}$ may be chosen as any point along the cable. The orientation of $\{C\}$ relative

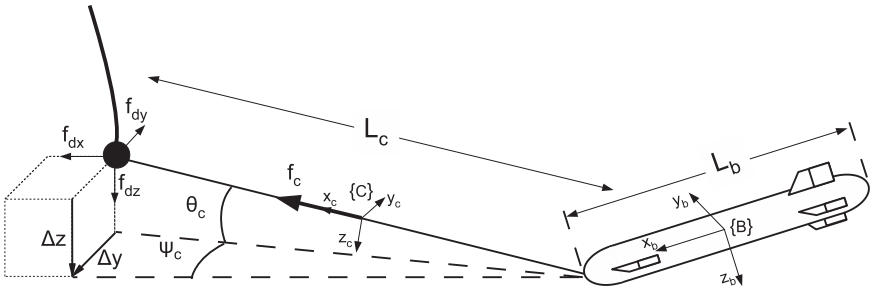

Fig. 3. External forces applied to the vehicle towing-point. Notice the orientation of the reference frames $\{B\}$ and $\{C\}$ relative to the inertial frame $\{I\}$ in which the distance vectors Δy and Δz, and the towing forces f_{dx}, f_{dy}, and f_{dz} are expressed.

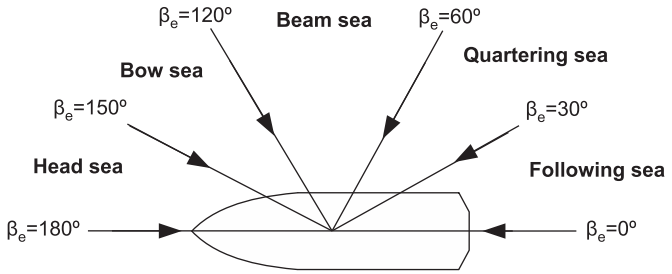

Fig. 4. Definition of encountering angle β_e and respective wave-aspects.

to $\{I\}$ is determined by a transformation defined by a sequence of two rotations: a rotation over yaw angle ψ_c about the z-axis followed by a rotation over pitch angle θ_c about y_c.

The forces applied to the depressor give rise to the force f_c along the cable, actuating at the towfish towing point according to the model presented in Appendix C; see Fig. 3. When the distance $|\Delta L|$ between the depressor and the towing point is smaller than the cable length L_c, the forces actuating at the depressor are not transmitted to the towed vehicle. This model is suitable to generate (realistic) impulsive forces that affect the stability of the towfish. Hence, the vector τ_e of external forces and moments expressed in the body-fixed referential is determined by

$$\tau_e := [\tau_{e_f}, \tau_{e_m}]',$$

where

$$\tau_{e_f} := \begin{cases} (R_B^I)^T R_C^I f_c & \Leftarrow |\Delta L| > L_c, \\ 0 & \Leftarrow |\Delta L| \le L_c, \end{cases}$$

$$\tau_{e_m} := [L_b/2, 0, 0]' \times \tau_{e_f},$$

with L_b denoting the length of the vehicle. R_C^I and R_B^I are the rotation matrices from $\{C\}$ to $\{I\}$ and from $\{B\}$ to $\{I\}$, respectively.

2.6.2. Modelling wave-driven disturbances

To capture a realistic scenario, the wave induced perturbations are modelled according to the JONSWAP wave spectrum (see e.g. Fossen, 2002). The spectral density function of the wave model used in the simulations is illustrated in Fig. 5. The peak frequency used in the model is computed as the frequency of encounter ω_e, defined by

$$\omega_e(u, \omega_0, \beta_e) := \left| \omega_0 - \frac{\omega_0^2}{g} u \cos\beta_e \right|,$$

where ω_0 is the modal frequency of the JONSWAP wave spectrum, u is the surge speed of the surface vessel, and β_e is the angle of encounter defined between the ship's heading and the direction of the incident waves; see Fig. 4. In this work, the towing vessel is assumed to be operated in head seas.

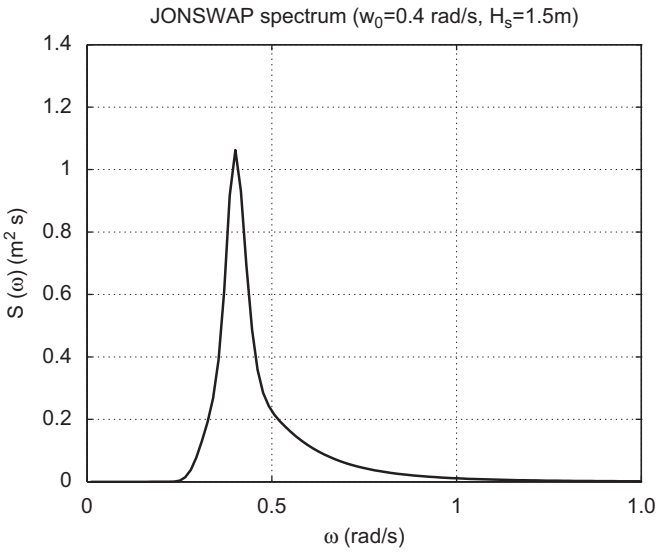

Fig. 5. JONSWAP wave spectrum used in the simulations. The specific wave spectrum used in each simulation is also a function of the towing speed.

The model adopted for wave-driven disturbances decomposes the ship motion that drives the oscillations of the gravitic depressor into three components of which heave is the most significant one. To implement this approach the sea wave amplitude determined by the JONSWAP wave model is decomposed into the three orthogonal components of motion and has a different phase delay associated to each direction. The relative motion amplitude in each direction is defined by the parameters r_x, r_y, and r_z and the corresponding phases are represented by ϕ_x, ϕ_y, and ϕ_z, respectively; see Table 6. The perturbation model used includes a low-frequency component in sway similar to that proposed by Wu and Chwang (2000). In modelling the heave component we take in consideration the experimental results obtained by Preston and Shupe (1993). These results show that the significant means of the towing vessel's vertical and horizontal displacements in head seas is nearly proportional to the significant wave height.

3. Control problem formulation

In this section we describe the dynamical model of the vehicle and formulate the problem of depth tracking and attitude control, in the presence of external disturbances and parametric model uncertainty. At a first stage the formulation is presented neglecting the motion in roll. The impact of the latter on the vehicle dynamics and control performance will be examined at a later stage. The coupling terms of the system dynamics resulting from the motion in roll will be introduced in Section 4.3.

3.1. Simplified equations of motion used for controller design

3.1.1. Kinematics

The pose (position and attitude) of the vehicle relative to $\{I\}$ is represented by vector $X_1 \coloneqq [z,\theta,\psi]'$. The velocity vector that includes heave velocity and *pitch* and *yaw* rates expressed in $\{B\}$ is $X_2 \coloneqq [w,q,r]'$. The simplified kinematic model based on the assumption that the vehicle is stable in *roll* is

$$\dot{z} = -u\sin\theta + w\cos\theta,$$

$$\dot{\theta} = q,$$

$$\dot{\psi} = r/\cos\theta. \tag{2}$$

3.1.2. Dynamics

The relevant equations of the simplified body-fixed dynamics are given by

$$\begin{aligned}&(\overline{m}-Z_{\dot{w}})\dot{w}-Z_{\dot{u}}\dot{u}-Z_{\dot{q}}\dot{q}-(\overline{m}-X_{\dot{u}})uq-Z_{|q|q}|q|q+f_w(v_1,\alpha,\beta)+g_w(\theta)\\&\quad=\overline{u}_w(v,\alpha,\delta)+\tau_w,\end{aligned} \tag{3}$$

$$\begin{aligned}&(I_{yy}-M_{\dot{q}})\dot{q}-M_{\dot{u}}\dot{u}-M_{\dot{w}}\dot{w}\\&\qquad+(Z_{\dot{w}}-X_{\dot{u}})uw-I_{xz}r^2-M_{|q|q}|q|q+f_\theta(v_1,\alpha,\beta)+g_\theta(\theta)\\&\quad=\overline{u}_\theta(v,\delta)+\tau_\theta,\end{aligned} \tag{4}$$

$$\begin{aligned}&(I_{zz}-N_{\dot{r}})\dot{r}-N_{\dot{v}}\dot{v}+(X_{\dot{u}}-Y_{\dot{v}})uv+I_{xz}rq-N_{|r|r}|r|r+f_\psi(v_1,\alpha,\beta)\\&\quad=\overline{u}_\psi(v,\beta,\delta)+\tau_\psi.\end{aligned} \tag{5}$$

where $\delta \coloneqq [\delta_b,\delta_s,\delta_r]'$ is the vector of deflections of the three control surfaces (bow, stern elevators, and rudder) and α and β represent the angles of attack and side-slip, defined as $\alpha \coloneqq \tan^{-1}(w/u)$ and $\beta \coloneqq \tan^{-1}(v/\sqrt{u^2+w^2})$, respectively. The variables τ_w, τ_θ, and τ_ψ denote external forces and moments resulting from the towing forces and external disturbances. The functions $\overline{u}_w(\cdot)$, $\overline{u}_\theta(\cdot)$, and $\overline{u}_\psi(\cdot)$ represent the forces and moments due to the common mode $(\delta_b+\delta_s)$, differential mode $(\delta_b-\delta_s)$, and rudder (δ_r) control actions, respectively. The remaining functions, $f_w(\cdot)$, $f_\theta(\cdot)$, and $f_\psi(\cdot)$, are hydrodynamic forces and moments associated with heave, *pitch* and *yaw*, respectively;$g_w(\cdot)$ and $g_\theta(\cdot)$ denote the restoring forces and moments. The constants $M_{\dot{q}}$,$M_{\dot{u}}$, $M_{\dot{w}}$, $N_{\dot{v}}$, $X_{\dot{u}}$, $Z_{\dot{q}}$, $Z_{\dot{u}}$, $Z_{\dot{w}}$, $M_{|q|q}$, $N_{|r|r}$, and $Z_{|q|q}$ represent system coefficients according to the notation of SNAME (1950). The meaning and values of the system's parameters are presented in Table 5.

3.1.3. Linearly parametrized system

To cast the system in the form of a linear parametric model, all the system parameters are lumped in matrix Γ which is derived below (refer to Tables 2–5 for the definitions of the vehicle parameters used in the forthcoming expressions). Define

$$a_1 \coloneqq \frac{1}{\overline{m}-Z_{\dot{w}}},$$

$$a_2 \coloneqq \frac{1}{(I_{yy}-M_{\dot{q}})},$$

$$a_3 \coloneqq \frac{1}{(I_{zz}-N_{\dot{r}})}, \tag{6}$$

$$\Gamma_1 \coloneqq a_1[Z_{|q|q},(\overline{m}-X_{\dot{u}}),\overline{V}^{2/3},(\overline{W}-\overline{B})]',$$

$$\Gamma_2 \coloneqq a_2[M_{|q|q},(X_{\dot{u}}-Z_{\dot{w}}),\overline{V},\overline{B},I_{xz}]',$$

$$\Gamma_3 \coloneqq a_3[N_{|r|r},V,-I_{xz}]', \tag{7}$$

and take $A \coloneqq \mathrm{diag}(a_1,a_2,a_3) > 0$. Consider also the following functions of the measured variables:

$$\sigma_1 \coloneqq [|q|q,uq,f_v(v_1)C_z(\alpha,\beta),\cos\theta]',$$

$$\sigma_2 \coloneqq [|q|q,uw,f_v(v_1)C_M(\alpha,\beta),z_B\sin\theta,r^2]',$$

$$\sigma_3 \coloneqq [|r|r,f_v(v_1)C_N(\alpha,\beta),rq]', \tag{8}$$

with $f_v(v_1) \coloneqq \frac{1}{2}\rho(u^2+v^2+w^2)$, $C_z(\alpha,\beta) \coloneqq -C_{L\alpha\beta}\alpha$, $C_M(\alpha,\beta) \coloneqq -C_{M\alpha\beta}\alpha$, and $C_N(\alpha,\beta) \coloneqq C_{M\alpha\beta}\beta$. Notice that the terms involving parameters $Z_{\dot{u}}$, $Z_{\dot{q}}$, $N_{\dot{v}}$, and $M_{\dot{u}}$ have been eliminated in the above expressions. These constants correspond to off-diagonal elements of the added-mass matrix that can be neglected (see Fossen, 2002). Using the above definitions and making $\Gamma \coloneqq \mathrm{diag}(\Gamma_1',\Gamma_2',\Gamma_3')$, $\Sigma \coloneqq [\sigma_1',\sigma_2',\sigma_3']'$, and $f \coloneqq \Gamma\Sigma$, the system dynamics (3)–(5) admit the representation

$$\dot{X}_2 = f + A\overline{u} + d, \tag{9}$$

where $d \coloneqq A[\tau_w,\tau_\theta,\tau_\psi]'$ represents the effect of the external forces and moments and the control actions are represented by $\overline{u} \coloneqq [\overline{u}_w,\overline{u}_\theta,\overline{u}_\psi]'$. The simplified kinematics are represented by

$$\dot{X}_1 = B^{-1}(X_2-g), \tag{10}$$

where $B \coloneqq \mathrm{diag}(1/\cos\theta,1,\cos\theta) > 0$ and $g \coloneqq [u\tan\theta,0,0]'$ with $|\theta| < \pi/2$.

3.2. Control problem formulation

Let $z_d : [0,\infty) \to \mathbb{R}$ be a sufficiently smooth time-varying depth reference trajectory with a uniformly bounded time-derivative and let the desired *pitch* and *yaw* angles be θ_d and ψ_d, respectively. Define also the tracking error as $\overline{e} \coloneqq X_1 - X_{1d} = [z-z_d,\theta-\theta_d,\psi-\psi_d]'$. The problem we address can be formally posed as follows:

Consider the state-space model

$$\dot{X}_1 = f_1(X_1,y_2), \quad y_1 = h_1(X_1,v_1)$$

$$\dot{X}_2 = f_2(X_2,y_1,u_e), \quad y_2 = h_2(X_2,v_1)$$

where $f_1(\cdot)$ denotes the kinematic model represented by (10), $f_2(\cdot)$ denotes the dynamic model represented by (9), y_1 and y_2 are the measured outputs, $h_1(\cdot)$ and $h_2(\cdot)$ denote measurement functions or observers, and u_e denotes the external forces affecting the system. Design an output-feedback control law such that all closed-loop signals are bounded and the tracking error norm $\|\overline{e}\|$ converges exponentially fast to a neighbourhood of the origin that can be made arbitrarily small in the presence of parameter model uncertainty and bounded external disturbances.

4. Output feedback controller design

To solve the trajectory tracking problem formulated above we propose a Lyapunov-based adaptive control law. Its derivation makes ample use of backstepping theory (see e.g. Khalil, 2002) and unfolds in the sequence of steps detailed below.

4.1. Nonlinear controller design

Step 1: Convergence of $\overline{e}$. Consider the Lyapunov control function $V_1 \coloneqq \frac{1}{2}\overline{e}'\overline{e}$, whose time-derivative is

$$\dot{V}_1 = (X_1-X_{1d})'(\dot{X}_1-\dot{X}_{1d}) = (X_1-X_{1d})'(B^{-1}(X_2-g)-\dot{X}_{1d}). \tag{11}$$

Using X_2 as a virtual control input and setting $X_2 = B(\dot{X}_{1d}-K_a\overline{e})+g$, for some positive definite (p.d.) diagonal matrix K_a makes $\dot{V}_1$ negative. Clearly, the desired trajectory represented by X_{1d} is required to be bounded and twice time-differentiable.

Define the error variable $\overline{z} \coloneqq X_2 - B(\dot{X}_{1d} - K_a\overline{e}) - g$. Then, (11) can be re-written as

$$\dot{V}_1 = -\overline{e}' K_a \overline{e} + \overline{e}' B^{-1} \overline{z}. \tag{12}$$

Step 2: Backstepping for z. For simplicity of presentation, assume at this stage that there are no external disturbances. This assumption will be removed later. Under these conditions, $d=0$ in (9). The dynamic equation of the error $\overline{z}$ can then be written as

$$\dot{\overline{z}} = f + A\overline{u} + B(K_a\dot{\overline{e}} - \ddot{X}_{1d}) + \dot{B}(K_a\overline{e} - \dot{X}_{1d}) - \dot{g}, \tag{13}$$

where $\ddot{X}_{1d}$ is the second time-derivative of the reference trajectory.

Define the augmented Lyapunov function

$$V_2 \coloneqq V_1 + \tfrac{1}{2}\overline{z}'\overline{z} = \tfrac{1}{2}\overline{e}'\overline{e} + \tfrac{1}{2}\overline{z}'\overline{z}. \tag{14}$$

Using (13), its time-derivative is

$$\dot{V}_2 = -\overline{e}' K_a \overline{e} + \overline{z}'[B^{-1}\overline{e} + f + A\overline{u} + B(K_a\dot{\overline{e}} - \ddot{X}_{1d}) + \dot{B}(K_a\overline{e} - \dot{X}_{1d}) - \dot{g}]. \tag{15}$$

The objective is to drive the term on $\overline{z}$ to zero using the control $\overline{u}$. However, this is not practical to do because some of the parameters of the vehicle are not known with good accuracy. Hence, the variables $\hat{a}_1$, $\hat{a}_2$, $\hat{a}_3$, $\hat{\Gamma}_1$, $\hat{\Gamma}_2$, and $\hat{\Gamma}_3$ are defined to represent estimates of a_1, a_2, a_3, Γ_1, Γ_2, and Γ_3, respectively, and set the control using the estimated model parameters as

$$\overline{u} \coloneqq -\hat{A}^{-1}[B^{-1}\overline{e} + \hat{f} + B(K_a\dot{\overline{e}} - \ddot{X}_{1d}) + \dot{B}(K_a\overline{e} - \dot{X}_{1d}) - \dot{g} + K_b\overline{z}], \tag{16}$$

where K_b is a p.d. diagonal matrix, $\hat{A} \coloneqq \mathrm{diag}(\hat{a}_1, \hat{a}_2, \hat{a}_3)$, and $\hat{f} \coloneqq \hat{\Gamma}\Sigma = \mathrm{diag}(\hat{\Gamma}_1', \hat{\Gamma}_2', \hat{\Gamma}_3')\Sigma$. It is required that $\ddot{X}_{1d}$ be bounded in order to guarantee boundedness of the control signal. Define also $\Pi \coloneqq [\Gamma, A]'$ and the estimation errors $\tilde{A} \coloneqq A - \hat{A}$, $\tilde{\Gamma} \coloneqq \Gamma - \hat{\Gamma}$, and $\tilde{\Pi} \coloneqq \Pi - \hat{\Pi}$ with $\hat{\Pi} \coloneqq [\hat{\Gamma}, \hat{A}]'$, and take $\Phi \coloneqq [\Sigma', -(\hat{A}^{-1}(\hat{\Gamma}\Sigma + B^{-1}\overline{e} + B(K_a\dot{\overline{e}} - \ddot{X}_{1d}) + \dot{B}(K_a\overline{e} - \dot{X}_{1d}) - \dot{g} + K_b\overline{z}))']'$. Using the control law (16), straightforward algebraic manipulations yield the time-derivative of V_2 as

$$\begin{aligned}\dot{V}_2 &= -\overline{e}' K_a \overline{e} - \overline{z}' K_b \overline{z} + \overline{z}'[\tilde{\Gamma}\Sigma - \hat{A}^{-1}\tilde{A}(\hat{\Gamma}\Sigma + B^{-1}\overline{e} + B(K_a\dot{\overline{e}} - \ddot{X}_{1d}) \\ &\quad + \dot{B}(K_a\overline{e} - \dot{X}_{1d}) - \dot{g} + K_b\overline{z})] \\ &= -\overline{e}' K_a \overline{e} - \overline{z}' K_b \overline{z} + \overline{z}'\tilde{\Pi}'\Phi.\end{aligned} \tag{17}$$

Step 3: *Adaptive control*. At this stage we introduce a third Lyapunov function that captures the effect of the error in the estimation of the system's parameters,

$$V_3 \coloneqq V_2 + \frac{1}{2m}\|\tilde{\Pi}\|_F^2 = \frac{1}{2}\overline{e}'\overline{e} + \frac{1}{2}\overline{z}'\overline{z} + \frac{1}{2m}\|\tilde{\Pi}\|_F^2 \tag{18}$$

for some scalar $m > 0$, where $\|\cdot\|_F$ stands for the Frobenius norm. The time-derivative of V_3 is

$$\dot{V}_3 = -\overline{e}' K_a \overline{e} - \overline{z}' K_b \overline{z} + \mathbf{tr}\left(\tilde{\Pi}'\left(\Phi\overline{z}' - \frac{1}{m}\dot{\hat{\Pi}}\right)\right). \tag{19}$$

Let $\hat{\Pi}_0$ represent an initial estimate of Π and let $\tilde{\Pi}_0$ be an upper bound on the error $\Pi - \hat{\Pi}_0$. Setting the dynamics of $\hat{\Pi}$ as

$$\dot{\hat{\Pi}} = m[\Phi\overline{z}' - n(\hat{\Pi} - \hat{\Pi}_0)] \tag{20}$$

for some scalar $n > 0$ yields

$$\dot{V}_3 = -\overline{e}' K_a \overline{e} - \overline{z}' K_b \overline{z} + \mathbf{tr}(n\tilde{\Pi}'(\hat{\Pi} - \hat{\Pi}_0)).$$

Note that the effect of the scalar gain n in the adaptive control law (20) is to ensure that the values of the system parameters estimated by the adaptive controller remain inside a ball with the center defined by the corresponding initial values. Applying the equality

$$\mathbf{tr}(n\tilde{\Pi}'(\hat{\Pi} - \hat{\Pi}_0)) = -\tfrac{1}{2}n\|\tilde{\Pi}\|_F^2 - \tfrac{1}{2}n\|\hat{\Pi} - \hat{\Pi}_0\|_F^2 + \tfrac{1}{2}n\|\Pi - \hat{\Pi}_0\|_F^2$$

yields

$$\dot{V}_3 \le -\overline{e}' K_a \overline{e} - \overline{z}' K_b \overline{z} - \tfrac{1}{2}n\|\tilde{\Pi}\|_F^2 + \tfrac{1}{2}n\|\tilde{\Pi}_0\|_F^2. \tag{21}$$

Although it is not possible to ensure that $\dot{V}_3$ is always negative, it is shown in the forthcoming analysis that this is sufficient to ensure practical stability (Jiang et al., 1994).

External forces. At this stage the simplifying assumption made in *Step* 2 is removed to consider the external forces and moments represented by d in (9). Noting that these are unknown terms that cannot be taken into account in the control law (16), instead of (17) it follows:

$$\dot{V}_2 = -\overline{e}' K_a \overline{e} - \overline{z}' K_b \overline{z} + \overline{z}'\tilde{\Pi}'\Phi + \overline{z}' d \tag{22}$$

and

$$\dot{V}_3 \le -\overline{e}' K_a \overline{e} - \overline{z}' K_b \overline{z} - \tfrac{1}{2}n\|\tilde{\Pi}\|_F^2 + \tfrac{1}{2}n\|\tilde{\Pi}_0\|_F^2 + \overline{z}' d. \tag{23}$$

4.2. Stability analysis

The following theorem may now be formulated:

Theorem I. *Consider the closed-loop system Ω consisting of the vehicle model* (2)–(5) *and the adaptive feedback controller* (13), (16), *and* (20). *Given a bounded, sufficiently smooth time-varying reference trajectory* $X_{1d} : [0,\infty) \to \mathbb{R} \times (-\pi/2, \pi/2) \times [-\pi, \pi]$, *the following holds*:

(i) *For any initial condition, the solution to Ω exists globally, all the closed-loop signals are bounded, and the tracking error $\overline{e}$ satisfies*

$$\|\overline{e}\| \le e^{-\lambda t}c_0 + \varepsilon, \tag{24}$$

where λ, c_0, and ε are positive constants and c_0 depends on the initial conditions.

(ii) *By appropriate choice of the controller parameter K_b, the rate of convergence λ and the radius ε can be chosen at will.*

Proof. From (23), using Young's inequality,[1] follows that

$$\dot{V}_3 \le -\overline{e}' K_a \overline{e} - \overline{z}'\left(K_b - \frac{\kappa}{2}I\right)\overline{z} - \frac{1}{2}n\|\tilde{\Pi}\|_F^2 + \frac{1}{2}\Delta^2, \tag{25}$$

for any scalar constant $\kappa > 0$, where $\Delta = d_b/\sqrt{\kappa} + \sqrt{n}\|\tilde{\Pi}_0\|_F$, with $d_b \coloneqq \sup_{t\ge 0}\|d\|$. From (18) and (25), and assuming that K_b satisfies $K_b > (\kappa/2)I$, we conclude that there exists a constant λ that verifies simultaneously $0 < \lambda \le mn$, $\lambda I \le K_a$, and $\lambda I \le 2K_b - \kappa I$, and therefore

$$\dot{V}_3 \le -\lambda V_3 + \tfrac{1}{2}\Delta^2. \tag{26}$$

Statement (i) is proven by applying the Comparison Lemma (Khalil, 2002) and showing that

$$V_3(t) \le e^{-\lambda t}V_3(0) + \frac{1}{2\lambda}\Delta^2 \tag{27}$$

along the solutions of Ω. This shows that all control signals remain bounded and the solutions of the system exist globally and are ultimately bounded with ultimate bound $(1/2\lambda)\Delta^2$. Considering the definition of V_3, we conclude from (27) that $\|\overline{e}\|$ converges to a ball of radius $\Delta/\sqrt{2\lambda}$. We can also conclude that the closed-loop system is input-to-state practically stable (ISpS) (Jiang et al., 1994) with respect to bounded parametric uncertainties and bounded external disturbances. To prove (ii) it is shown that the radius $\Delta/\sqrt{2\lambda}$ can be made arbitrarily small by appropriate choice of the controller parameters. For a given limiting radius ε and a

[1] Young's inequality states that if a and b are non-negative real numbers and p and q are positive real numbers such that $1/p + 1/q = 1$ then $ab \le a^p/p + b^q/q$. In particular, for any real number $\varepsilon > 0$ $ab \le a^2/2\varepsilon + \varepsilon b^2/2$.

given convergence rate λ

$$\frac{\Delta}{\sqrt{2\lambda}} \le \varepsilon = \frac{d_b}{\sqrt{2\lambda\kappa}} + \sqrt{\frac{n}{2\lambda}}\|\tilde{\Pi}_0\|_F,$$

and it is possible to make

$$\kappa := d_b^2/2\lambda\left(\varepsilon - \sqrt{\frac{n}{2\lambda}}\|\tilde{\Pi}_0\|_F\right)^2$$

provided that

$$K_b - \frac{\kappa}{2}I = K_b - \frac{d_b^2}{2\lambda\left(\varepsilon - \sqrt{\frac{n}{2\lambda}}\|\tilde{\Pi}_0\|_F\right)^2}I \ge \frac{\lambda}{2}I > 0.$$

Thus, it is shown that (26) is verified and therefore (27) holds.

4.3. Coupling the horizontal and vertical planes

To take in account the effects of motion in *roll*, the following coupling terms must be inserted in the dynamic equations of the system (see Appendix D):

$$\Gamma_{c1} := a_1[-(\overline{m}-Y_{\dot v}),(\overline{W}-\overline{B})]',$$

$$\Gamma_{c2} := a_2[(I_{zz}-I_{xx}+K_{\dot p}-N_{\dot r}),-I_{xz}]',$$

$$\Gamma_{c3} := a_3[(I_{xx}-I_{yy}+M_{\dot q}-K_{\dot p}),I_{xz}]',$$

$$\sigma_{c1} := [vp,\cos\theta(\cos\phi-1)]',$$

$$\sigma_{c2} := [pr,p^2]', \quad \sigma_{c3} := [pq,p^2]'.$$

The system dynamics can be reformulated by substituting the new expressions for Γ, Σ, B, and g as follows. Define

$$\Gamma := \mathrm{diag}([\Gamma_1',\Gamma_{c1}'],[\Gamma_2',\Gamma_{c2}'],[\Gamma_3',\Gamma_{c3}']),$$

$$\Sigma := [\sigma_1',\sigma_{c1}',\sigma_2',\sigma_{c2}',\sigma_3',\sigma_{c3}']',$$

$$B := \mathrm{diag}(b_1+b_{c1},1+b_{c2},1/b_1+b_{c3}), \quad g := [g_1+g_{c1},g_{c2},g_{c3}]',$$

with $b_1 := 1/\cos\theta$, $g_1 := u\tan\theta$, $b_{c1} := (1-\cos\phi)/\cos\theta\cos\phi$, $b_{c2} := (\cos\phi-1)/\cos\phi$, $b_{c3} := \cos\theta(1-1/\cos\theta)$, $g_{c1} := u\tan\theta(1/\cos\theta-1)-v\tan\phi$, $g_{c2} := r\tan\phi$, and $g_{c3} := -q\tan\phi$. Let the coupling components of the system dynamics be represented by

$$\Omega_c := [\Gamma_{c1}'\sigma_{c1}+g_{c1},\Gamma_{c2}'\sigma_{c2}+g_{c2},\Gamma_{c3}'\sigma_{c3}+g_{c3}]' \tag{28}$$

and let b_u, b_v, and b_p denote the upper bounds on the surge and sway velocities, and roll rate, respectively. Simple algebraic manipulations show that

$$\|\Omega_c\|^2 \le C_c\|X_2\|^2 + \Delta_c, \tag{29}$$

where C_c and Δ_c are constants defined from the system parameters and the upper bounds on the linear velocities, b_u, b_v, and b_p (cf. Appendix D).

Inserting in (22) the coupling terms not compensated by the control $\overline{u}$ we obtain

$$\dot V_2 = -\overline{e}'K_a\overline{e} - \overline{z}'K_b\overline{z} + \overline{z}'\tilde{\Pi}'\Phi + \overline{z}'d + \overline{z}'\Omega_c. \tag{30}$$

Furthermore, applying Young's inequality we conclude from (25) that, for any scalar constant $\kappa_c > 0$, $\dot V_3$ verifies

$$\dot V_3 \le -\overline{e}'K_a\overline{e} - \overline{z}'\left(K_b - \frac{(\kappa+\kappa_c)}{2}I\right)\overline{z} - \frac{1}{2}n\|\tilde{\Pi}\|_F^2 + \frac{C_c}{2\kappa_c}\|X_2\|^2 + \nabla, \tag{31}$$

where $\nabla = \frac{1}{2}(\Delta^2 + \Delta_c/\kappa_c)$. It can be shown, applying a reasoning similar to the one used in Theorem 1, that

$$V_3(t) \le e^{-\lambda t}V_3(0) + \gamma_c(\|X_2\|) + \frac{\nabla}{\lambda}, \tag{32}$$

where γ_c is a class K function (Khalil, 2002); see demonstration in Appendix D. Hence, we conclude that the system is ISpS with respect to bounded unmodelled dynamics.

5. Nonlinear observer design

In actual implementations it is often impractical to obtain direct measurements of surge, sway, and heave for feedback. Taking this in consideration, for observer design purposes it is assumed that the surge velocity of the towed vehicle is constant and can be approximated by the nominal towing speed, i.e. $u := u_0$. Furthermore, the effect of the sway component is assumed to be negligible. The heave component of the vehicle's velocity is estimated by a nonlinear observer that is described below.

Consider the state space representation

$$H\dot x_o = F_\theta x_o + f_o(\theta,q,\tau_w) + g_o(x_o,\delta),$$

$$y_o = z, \tag{33}$$

where $x_o := [z,w]'$, $H := \mathrm{diag}(1,M_{3,3})$, $F_\theta := \left[\begin{smallmatrix}0 & \cos\theta \\ 0 & C_v\end{smallmatrix}\right]$,

$$f_o(\theta,q,\tau_w) := \begin{bmatrix} -u_0\sin\theta \\ (\overline{m}-X_{\dot u})u_0 q + Z_{|q|q}|q|q + (\overline{W}-\overline{B})\cos\theta + \tau_w \end{bmatrix},$$

and $g_o(x_o,\delta) := [0,-\frac{1}{2}\rho S_s C_{L\alpha}(u_0^2+w^2)\delta_c]'$, with $\delta_c := \delta_b + \delta_s$, $M_{3,3} := \overline{m}-Z_{\dot w} > 0$, and $Cv := -\frac{1}{2}\rho(\overline{V}^{2/3}C_{L\alpha\beta} + 2S_sC_{L\alpha})(u_0+0.3) < 0$. The variable τ_w represents the heave component of the external forces actuating on the towfish; see Section 3.1. Let $\hat z$ and $\hat w$ represent the estimated values of z and w, respectively, and define $\tilde w := w - \hat w$. Here we use the approximation $f_v(v_1)C_z(\alpha,\beta) \approx -\frac{1}{2}\rho C_{L\alpha\beta}(u_0+0.3)w$ that is justified in Appendix E.Applying the expression for the dynamics of w derived from (3) we implement an estimator of w in the form of a Luenberger observer

$$H\dot{\hat x}_o = F_\theta\hat x_o + f_o(\theta,q,\tau_w) + g_o(\hat x_o,\delta) + K_o(y_o - \hat y_o),$$

$$\hat y_o = h'\hat x_o = \hat z, \tag{34}$$

where $h := [1,0]'$ and $K_o := [k_1,k_2]'$ is the gain of the observer, with the scalars k_1 and k_2 defined in the sequel of the present formulation. In our implementation, due to the configuration of the towfish and the towing arrangement, the magnitude of τ_w is very small relatively to the remaining terms in $f_o(\cdot)$ and can be neglected. Using $\tilde x_o := x_o - \hat x_0$, $\delta_o := -\frac{1}{2}\rho S_s C_{L\alpha}\delta_c$, and $\tau_o := g_o(x_o,\delta) - g_o(\hat x_o,\delta) = [0,\delta_o(w^2-\hat w^2)]'$ the observer error dynamics become

$$H\dot{\tilde x}_o = F_\theta\tilde x_o - K_o h'\tilde x_o + \tau_o. \tag{35}$$

Introduce now the Lyapunov function $V_o := \tilde x_o' H\tilde x_o$. Its time derivative is

$$\dot V_o = -\tilde x_o' A_o\tilde x_o + 2\tilde x_o'\tau_o, \tag{36}$$

with $A_o := (K_o h' + hK_o' - F_\theta - F_\theta') > 0$ for all $k_1 > 0, k_2 \ge 1$.

The heave velocity of the vehicle is assumed to be bounded. This assumption is a natural consequence of the towing arrangement and towfish configuration and is validated by the results of simulations. In fact, even when the system is subjected to fast heave movements of the depressor, the towfish tends to pitch rather than heave. Given an upper bound b_w on $|w|$, it is straightforward to show that (see Appendix E)

$$\dot V_o = -\tilde x_o' A_o\tilde x_o + 2\delta_o\tilde w^2(w+\hat w) \le -\tilde x_o'[A_o - 2|\delta_o(b_w+\hat w)|I]\tilde x_o. \tag{37}$$

Notice that except for the diagonal element $a_{22} > 0$ the elements a_{ij} $(i,j=1,2)$ of matrix A_o are determined by the observer gains k_1 and k_2. Hence, to make $A_o - 2|\delta_o(b_w+\hat w)|I > 0$ the following

condition must hold:

$$|\delta_o(b_w+\hat{w})| < |C_v|. \tag{38}$$

Condition (38) establishes the region of attraction of the origin of $\tilde{x}_o$, which depends on the towing velocity as shown in Appendix E. Thus, although it is not possible to ensure global stability, through proper manipulation of the values of k_1 and k_2 the origin of $\tilde{x}_o$ can be made semi-globally asymptotically stable (Khalil, 2002).

5.1. Stability of the observer with respect to measurement noise

Consider now that the measurements of the variable z are affected by noise with bounded intensity. Let $\xi_z=[n_z,0]'$ be a noise vector. Substituting $y_o=z+n_z$ for the measurement expression in (33) leads to

$$\dot{V}_o=-\tilde{x}_o'A_o\tilde{x}_o+2\tilde{x}_o'(\tau_o-K_oh'\xi_z).$$

Using Hölder and Young's inequalities, appropriate algebraic manipulations show that

$$\dot{V}_o\le-\tilde{x}_o'[A_o-(2|\delta_o(b_w+\hat{w})|+\eta_on_z)I]\tilde{x}_o+\frac{|n_z|}{\eta_o}\|K_o\|^2,$$

where the constant $\eta_o>0$ can be made arbitrarily large provided that $A_o-(2|\delta_o(b_w+\hat{w})|+\eta_on_z)I>0$. Under this condition, a sufficiently small constant $\lambda_o>0$ exists such that

$$V_o(t)\le e^{-\lambda_ot}V_o(0)+\frac{\Delta_o}{\lambda_o}, \tag{39}$$

with $\Delta_o=(b_z/\eta_o)\|K_o\|^2>0$ and $b_z=\sup_{t\ge0}|n_z|$. Hence, we conclude that the observer is ISpS with respect to bounded measurement noise.

5.2. Stability of observer-controller

To analyse the stability of the controller with respect to bounded errors in the estimation of w we observe that the noise affecting variables u and w in (8) verifies the matching condition; that is, the uncertain terms enter the state equation (9) at the same point as the control input. Since the intensity of the noise is bounded and the variables w and u are also assumed to be bounded, the noisy effects in w can be regarded as additional bounded external disturbances. Hence, it is concluded from the previous analysis that the controller is ISpS with respect to bounded errors in the estimation of w.

Consider now the cascade system constituted by the observer f_L represented by (34) and the controller f_Ω represented by (13), (16), (20) as follows:

$$\dot{x}_1=f_\Omega(x_1,y_2,u_1),\quad y_2=x_2,$$

$$\dot{x}_2=f_L(x_2,u_2), \tag{40}$$

where $x_1:=\bar{e}$ represents the tracking error of the controlled system, $x_2:=\tilde{x}_o$ is the estimation error of the observer, the input $u_1:=\tau_e+\Omega_c$ represents the external disturbances plus the effect of unmodelled dynamics affecting f_Ω, and $u_2:=n_z$ represents the bounded noise input to the observer. Both the x_1 and x_2 subsystems with (y_2,u_1) and u_2, respectively, as inputs are ISpS. Hence, it is shown by application of the Generalized Small-Gain Theorem (Jiang et al., 1994) that the cascade system is ISpS with respect to bounded external disturbances and bounded noise in the depth measurements used by the observer; see Appendix E.

6. Results of simulations and discussion

The performance of the control algorithms developed is illustrated using the results of computer simulations. The initial conditions and other parameters which are common to all the simulations are presented in Table 6. The specific parameters of each simulated test are presented in Table 7. The reference depth profiles used in the simulations are shown in Fig. 6. In depth tracking simulations $z_d(t)$ is approximated by cubic-splines, thus ensuring that the reference trajectory is twice differentiable in time.

6.1. Simulations setup

In the scenario used for simulations the towed vehicle is required to regulate the pitch angle and the yaw error to zero while tracking a desired depth. Three types of depth trajectories were used: a real bathymetric profile with a total length of approximately 800 m, a sinusoidal reference, and a constant depth trajectory; see Fig. 6. In all trajectories the depressor is assumed to be deployed at an approximately constant depth with oscillations in position that are imposed by the motion of the

Table 7
Simulations' parameters by test number.

Test num.	Depth profile	Towing speed (knts)	Pigtail length (m)	Other conditions
1	Const. depth	4	100	Undisturbed; non-controlled
2	Const. depth	4	100	Non-controlled
3	Const. depth	4	50	Non-controlled
4	Const. depth	4	30	Non-controlled
5	Const. depth	3	100	–
6	Const. depth	4	100	–
7	Const. depth	6	100	–
8	Const. depth	8	100	–
9	Const. depth	6	50	–
10	Const. depth	6	30	–
11	Sinusoidal	6	100	Initial 100% estimation error of parameters a_1, a_2, a_3
12	Sinusoidal	6	100	Initial 100% estimation error of parameters a_1, a_2, a_3; without adaptive control
13	Bottom following	4	100	–
14	Bottom following	8	100	–
15	Sinusoidal	3	100	–
16	Sinusoidal	3	30	–
17	Const. depth	8	100	Subjected to ocean current with a velocity of 1 knt
18	Const. depth	10	100	Subjected to ocean current with a velocity of 1 knt
19	Const. depth	12	100	Subjected to ocean current with a velocity of 1 knt
20	Const. depth	8	50	Subjected to ocean current with a velocity of 1 knt

towing vessel at the sea surface. In the simulations, the towing system starts from rest and reaches the nominal towing speed. The operation of the system is simulated with towing speeds varying from 3 to 8 knts, using pigtail lengths of 30, 50, and 100 m. The actual towing velocity used in simulations has a bias of $\pm 10\%$ the nominal velocity. This is used to account for the difficulty of maintaining a specified towing speed of the support ship. The wave induced perturbations are modelled according to the JONSWAP wave spectrum considering a sea-state of 3–4; see Table 6. Notice that the spectral density function of the wave-driven perturbations as defined in Section 2.6.2 is also a function of the towing speed.

To investigate the robustness of the controlled system under the effect of non-measured ocean currents we consider an additional scenario where an underwater current with a velocity of 1 knt makes the towfish drift sideways and diverge from the desired track. The control system was simulated in this scenario with distinct system parameters and different towing velocities; see Table 7.

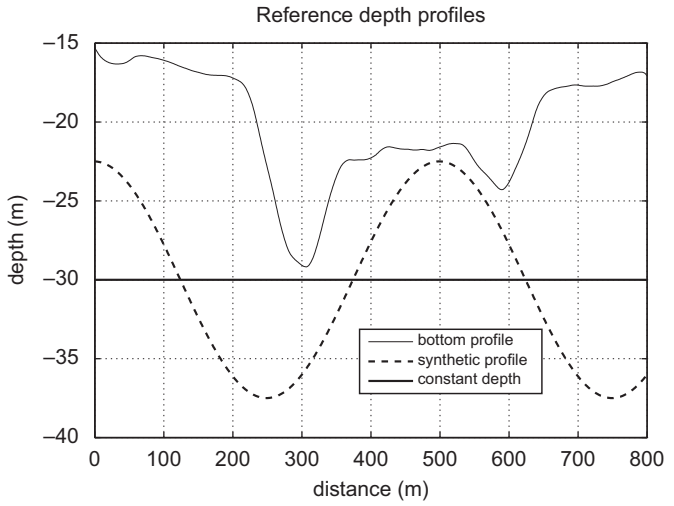

Fig. 6. Reference depth profiles used in simulations. Depths are represented by negative values to facilitate the visualization of the depth profile.

6.1.1. System's parameters and constraints

The initial estimates of the model parameters represented by Π_0 are set to $\pm 10\%$ of the corresponding true values. The exceptions to this rule are indicated in Table 7. The control planes have a maximum deflection of ± 30 deg and the actuators' dynamics are approximated by a first order system with a time constant equal to 0.1 s.

6.1.2. Measurement noise

To test the robustness of the proposed adaptive controller with respect to sensor noise, the measurements of z, θ, ψ, q, and r used in the simulations are affected by mutually independent additive Gaussian white noise whose standard deviations are represented by the constants σ_z, σ_θ, σ_ψ, σ_q, and σ_r, respectively; see the values of these constants in Table 6. We notice that, when operating close to the surface, depth measurements may be affected by pressure variations induced by sea waves. Although this problem has not been addressed in the study, we propose to filter these variations by fusing the depth sensor measurements with the altitude measurements obtained with a sonar altimeter.

6.2. Results and discussion

6.2.1. Depressor and towfish motions

The simulations reproduce closely the motion behaviour of the depressor determined by Chapman (1982): when the wave induced forces become nearly periodic the locus of the depressor in the vertical plane approximates an ellipse with the length of the major axis proportional to the vertical displacement of the ship and the minor axis one order of magnitude smaller; see Fig. 7. The plot of depressor and towfish motions shown in Fig. 10 is representative of the system motion with other pigtail lengths and towing speeds. These results show that the amplitude of surge and sway motions is not attenuated by the pigtail but heave motion is significantly reduced. This is in accordance with the experimental results cited in Section 2.3. However, our model

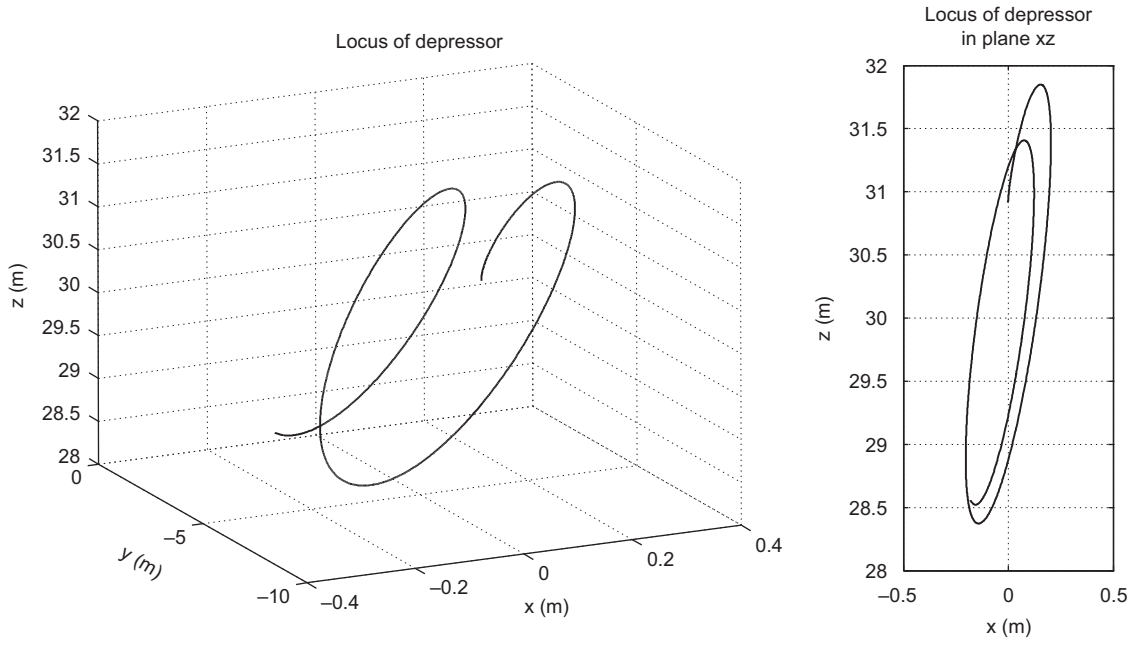

Fig. 7. Locus of the gravitic depressor corresponding to a nearly periodic motion of the towing vessel with lateral motion and zero surge speed.

shows low amplitude, high-frequency oscillations of the towfish towing point that are not reported in the cited works (see e.g. Fig. 10). This may be explained by the higher frequency contents of the sea-wave driven oscillations that are assumed to be transmitted to the depressor without attenuation and also by the intrinsic towfish oscillations that can be observed in Fig. 8. This natural oscillation of the towfish is inherent to the configuration with a small positive buoyancy.

6.2.2. Performance of the non-controlled system

The errors observed with the undisturbed, non-controlled system towed at constant depth are shown in Fig. 8. The towing speed is 4 knts; see the configuration of Test num. 1 in Table 7. The errors obtained with the non-controlled system subjected to wave-driven disturbances with a towing speed of 4 knts at constant depth are plotted in Fig. 9; see the configuration of Test num. 2 in Table 7. The external forces applied to the towfish are derived from the relative motions of depressor and towfish that are plotted in Fig. 10. These simulations show that the heave velocity of the non-controlled system is approximately zero. Corroborating the results of Preston (1992), the results illustrated in Fig. 9 show that yaw motion of the towed vehicle is not reduced with the two-part tow method.

6.2.3. System performance in constant-depth tracking and attitude control

The results presented in Figs. 11–15 illustrate the performance of the system subjected to the same external disturbances of the previous tests but under the control laws derived in Section 4.1. Fig. 13 presents the attitude of the vehicle in roll. These results show that the motion of the controlled vehicle is in accordance with our previous assumption of negligible motion in roll. The actuation of the control surfaces is depicted in Fig. 15. Notice that when towed at 4 knts the control surfaces' deflections are far from the saturation value. Fig. 14 shows that the estimation error achieved by the observer of w is very small and remains inside the region of attraction established in Appendix E. This error decreases significantly with increasing towing speeds.

6.2.4. Bottom following performance

The performance of the simulated system tracking the real bathymetric profile shown in Fig. 6 is illustrated in Figs. 16–19. A plot of the roll angle is presented in Fig. 17. Noting that bottom following is the most demanding scenario, we observe that by towing the vehicle at the velocity of 4 knts the depth and *pitch* errors verify

$$|\bar{e}_z| \leq 0.3\,\text{m},$$

$$|\bar{e}_\theta| < 1\,\text{deg},$$

the 2σ interval of the yaw error corresponds to

$$|\bar{e}_\psi| < 0.9\,\text{deg},$$

and the roll angle verifies

$$|\phi| < 0.25\,\text{deg}.$$

Notice that the tracking errors obtained in bottom-following missions increase considerably with increasing towing speed; compare the results of Test num. 13 and 14 plotted in Figs. 16 and 20, respectively. Hence, for this type of mission the recommended maximum towing speed is 4 knts.

6.2.5. Impact of pigtail length and towing speed on system performance

The impact of the length of the secondary cable on the tracking errors obtained with the controlled system is summarized by the plot of the RMS errors shown in Fig. 21. The depth tracking error decreases slightly with the increase of the pigtail length. For practical purposes, however, the impact of the latter is not significant. To assess the impact of the pigtail length when the main towing forces are not aligned with the vehicle longitudinal axis we simulated the system using the sinusoidal trajectory represented in Fig. 6 at a towing speed of 3 knts (tests num.

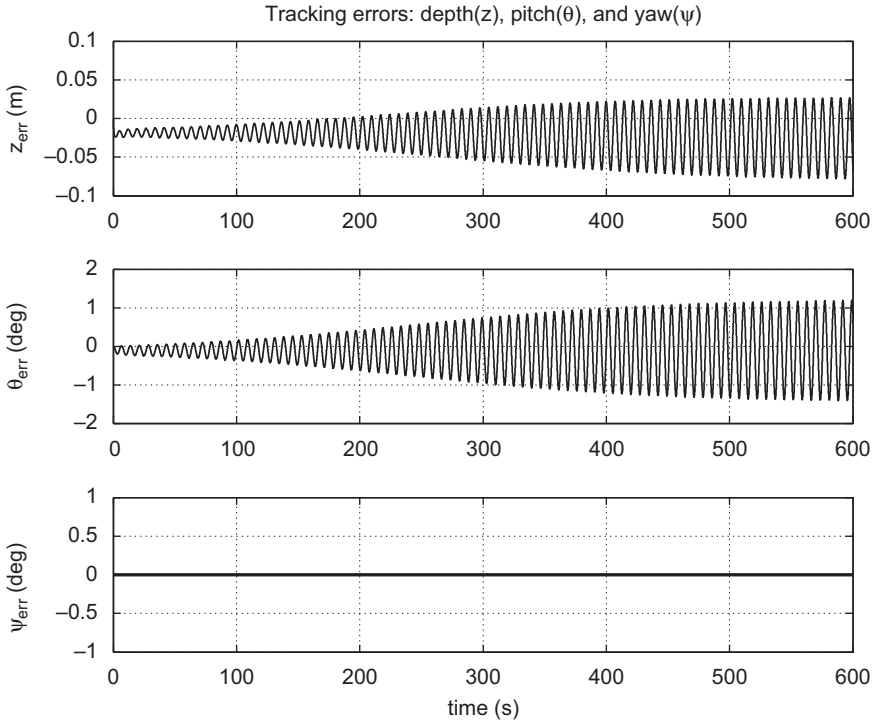

Fig. 8. Response of the undisturbed non-controlled system, towed at 4 knts (Test num.1).

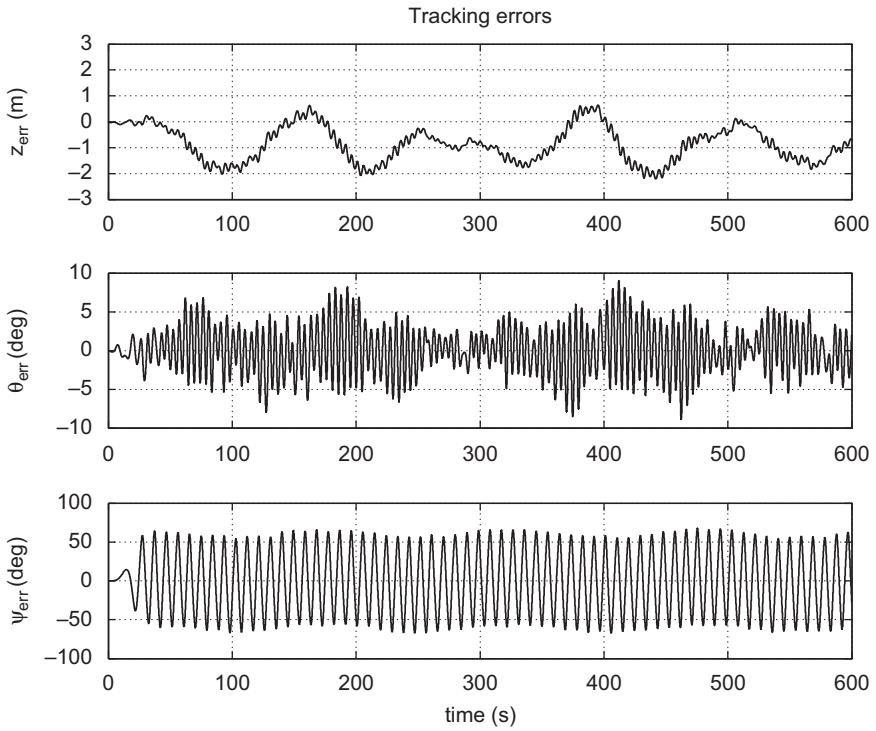

Fig. 9. Tracking errors obtained with the disturbed, non-controlled system towed at 4 knts; constant depth (Test num. 2). Compare these results with those obtained with the controlled system, in Fig. 11.

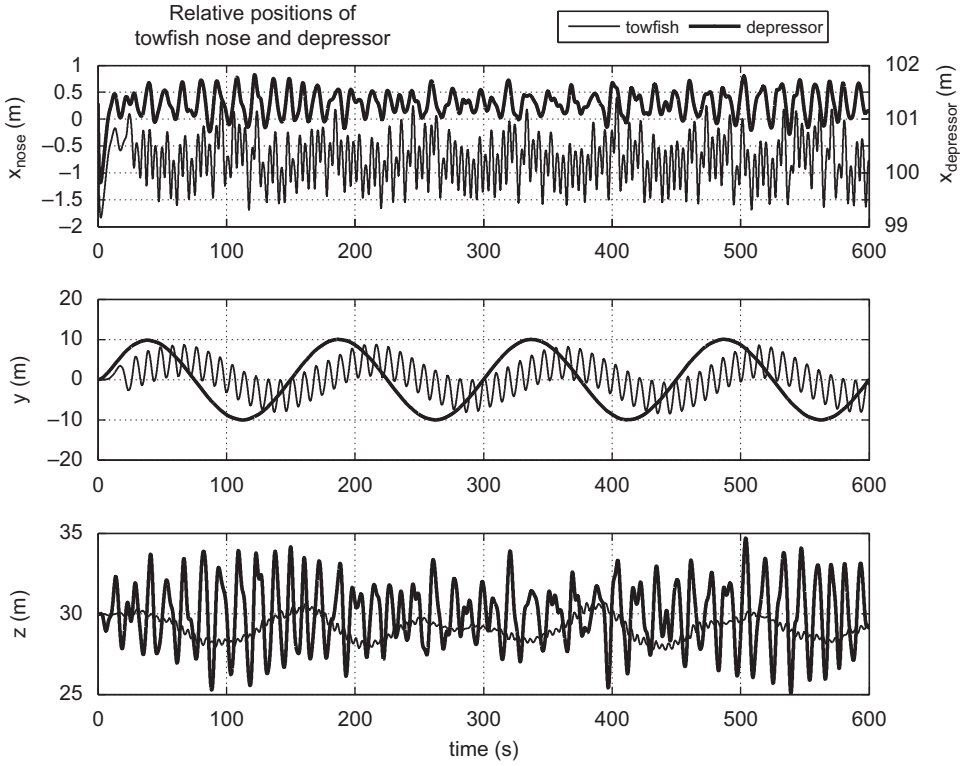

Fig. 10. Relative positions of depressor and towfish nose for the non-controlled system towed at 4 knts; constant depth (Test num. 2).

15 and 16). The errors obtained are similar to those obtained in the other simulations at comparable speeds. From these results we conclude that with this towing model the depth and pitch tracking errors of the controlled system are not practically affected by pigtail length. However, there is a significant impact on surge speed and lateral motion of the towfish, cf. Figs. 23 and 24. As a consequence, to mitigate accelerations in surge or lateral oscillations of the towfish position a longer pigtail is recommended.

The impact of different towing speeds on the performance of the controlled system is summarized in Fig. 22. These results

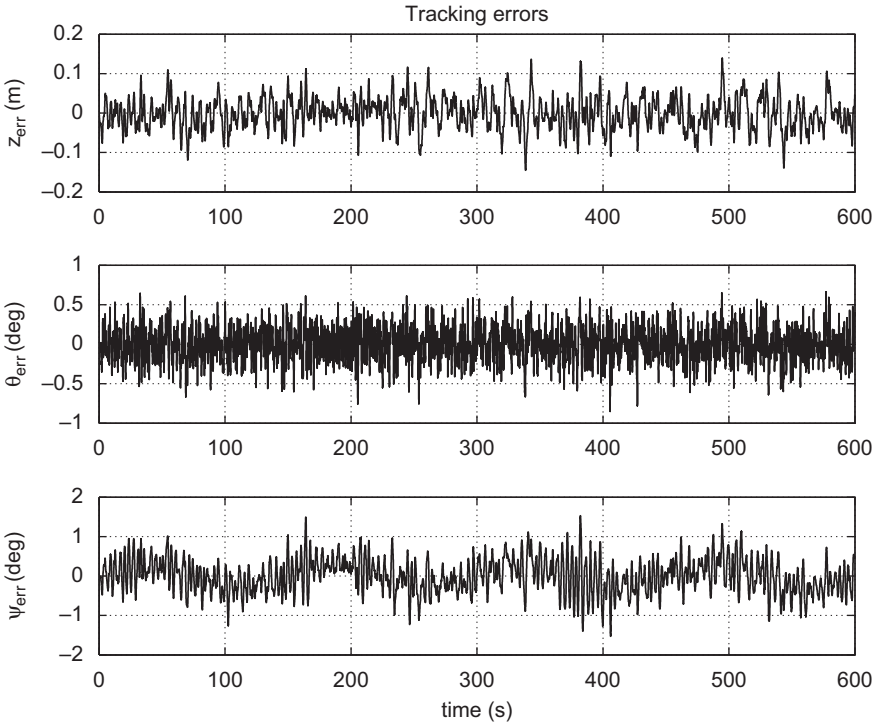

Fig. 11. Tracking errors obtained with the controlled system towed at 4 knts; constant depth trajectory (Test num.6). Compare these results with those obtained with the non-controlled system, in Fig. 9.

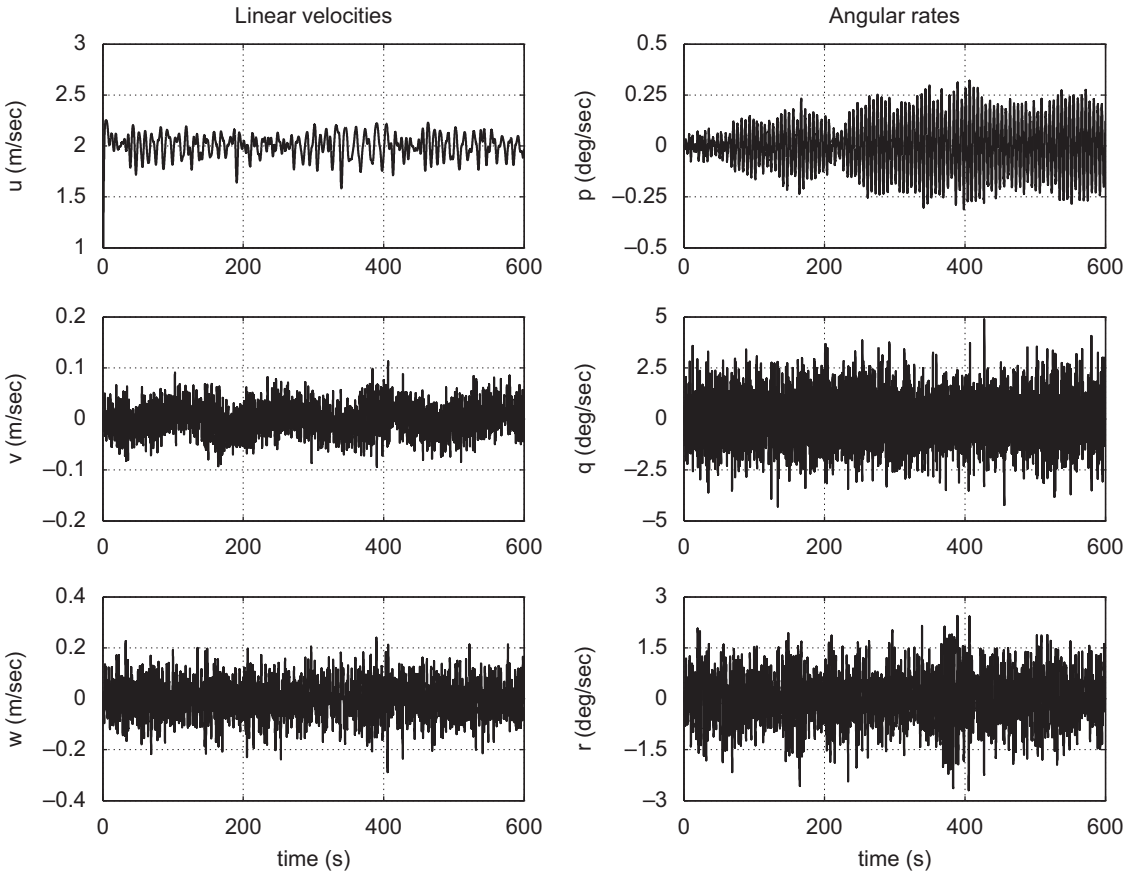

Fig. 12. Linear and angular velocities of the controlled system towed at 4 knts; constant depth trajectory (Test num. 6).

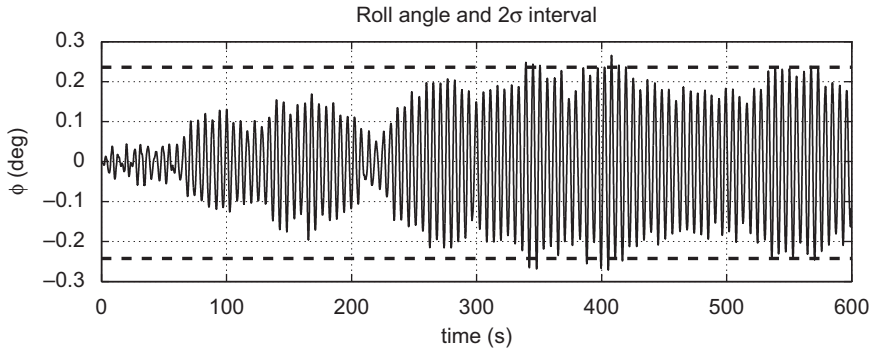

Fig. 13. Roll angle of the controlled towfish at 4 knts towing speed, constant depth trajectory (Test num. 6).

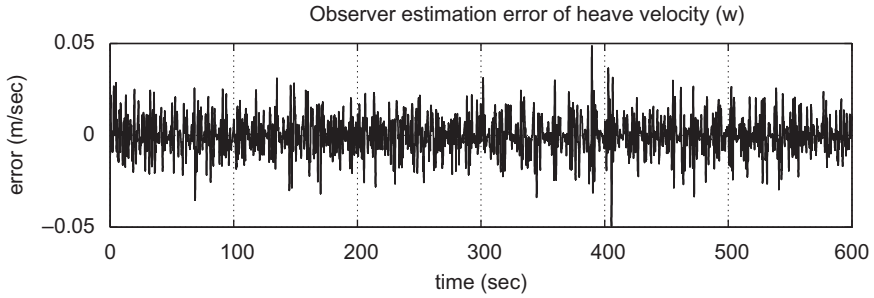

Fig. 14. Error in the estimation of heave velocity at 4 knts towing speed, constant depth trajectory (Test num. 6).

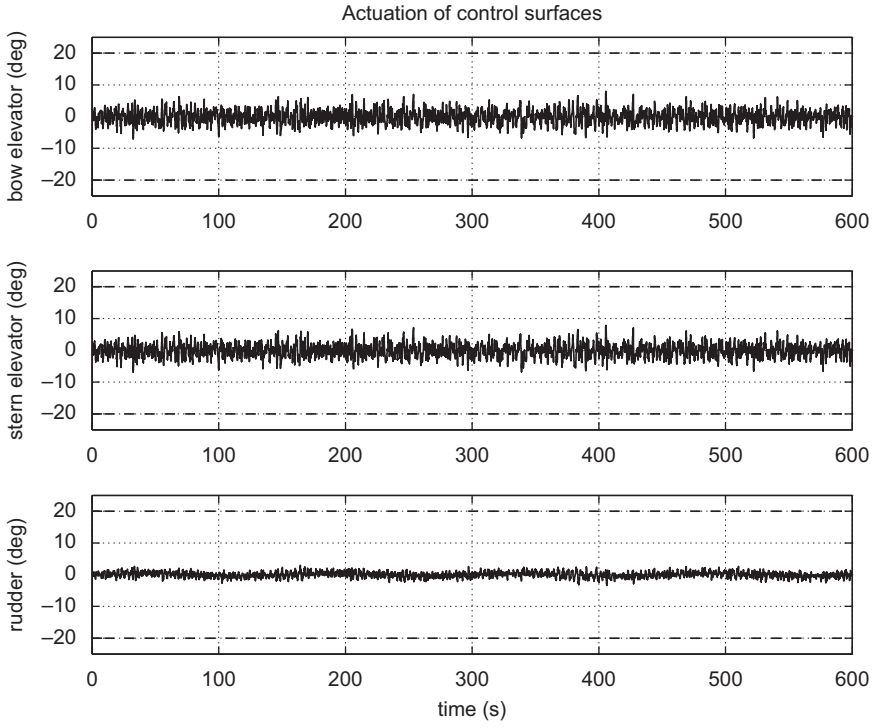

Fig. 15. Actuation of the control surfaces of the towfish at 4 knts towing speed, constant depth trajectory. The upper and lower dashed lines represent the hard-limits of deflection (Test num. 6).

indicate that for constant depth-tracking the depth and attitude errors increase slightly with increasing towing speed. This effect becomes more pronounced for speeds above 6 knts but even at this speed the tracking errors remain inside the limits specified for the system. It is observed in simulations that the error in yaw is the most variable both with towing speed and pigtail length although its RMS value remains smaller than 1 deg. For critical applications it may be convenient to use lower towing speeds and larger pigtail lengths. It is also important to notice, however, that at lower towing speeds the system is more susceptible to generate impulsive forces in the pigtail that can affect the stability of the system. This effect is illustrated in Fig. 25.

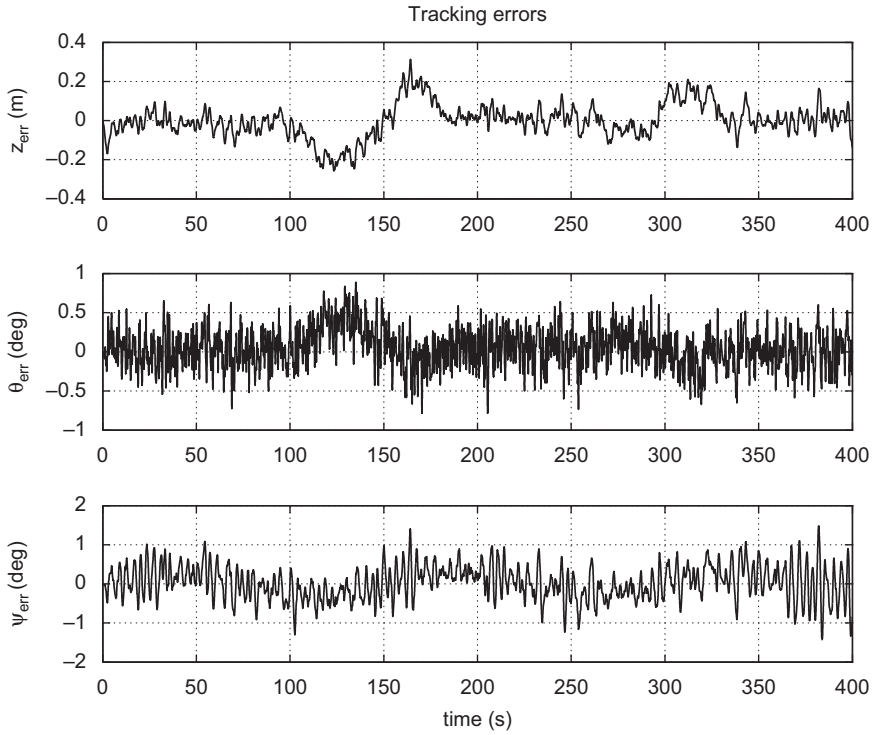

Fig. 16. Tracking errors in a bottom-following mission at 4 knts towing speed (Test num. 13).

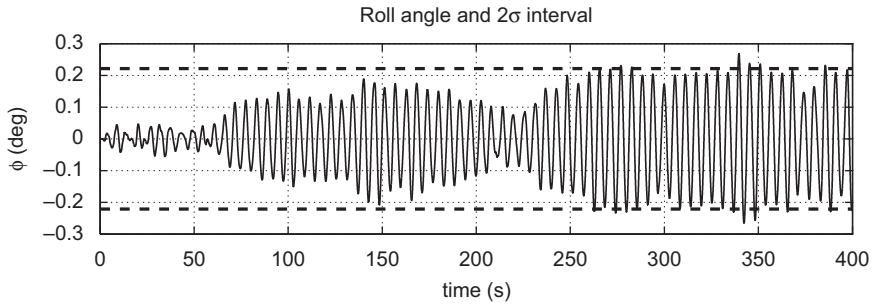

Fig. 17. Roll angle of the controlled towfish at 4 knts towing speed in a bottom-following mission (Test num. 13).

6.2.6. Adaptive controller

The importance of adaptive control can be assessed based on a comparison of the tracking errors obtained with and without parameter adaptation, as shown in Fig. 26(a) and (b). The plots correspond to Tests num. 11 and 12, respectively. These results show that adaptive control improves considerably the performance of the controller, especially in terms of depth tracking, when the error in the initial estimate of the parameters is large. It is shown that adaptive control may be fundamental to bound the tracking errors according to the system's specifications. Parameter estimation implemented in the adaptive controller is illustrated in Fig. 27 for parameters a_1, a_2, and a_3.

6.2.7. Performance in the presence of ocean currents

To analyse the performance of the controlled system in the presence of ocean currents several simulations were done including the effect of a current with a velocity of 1 knt that causes lateral drift of the towfish. The behaviour of the system in this scenario is illustrated in Figs. 28–31. Due to the geometry of the towing arrangement the external forces transmitted by the pigtail tend to affect directly the orientation of the vehicle as shown in the plots of Fig. 28. The control effort required in this scenario is shown in Fig. 29; notice that the rudder deflection becomes close to the hard limit of -30 deg. The tracking errors achieved by the system are shown in Fig. 30. Comparison of these errors with those achieved in the previous tests (see e.g. Fig. 11) shows that depth and pitch errors are not affected by the presence of the ocean current. In this test the amplitude of the yaw oscillations does not increase but the final orientation error has a bias of -1 deg. The motion in roll remains negligible.

The results obtained in simulations with a pigtail of 50 m show that although the time response of the system varies with pigtail length, the amplitude of the tracking errors is equivalent to that obtained with a larger cable; see Fig. 31. The simulations executed with towing speeds of 8, 10, and 12 knts show that for this range of velocities the amplitude of the error caused by the ocean current does not vary with towing speed.

7. Conclusions and future work

The paper addressed the problem of controlling an underwater towed vehicle in the vertical and horizontal planes. The system analysed consisted a two-stage towing arrangement that includes

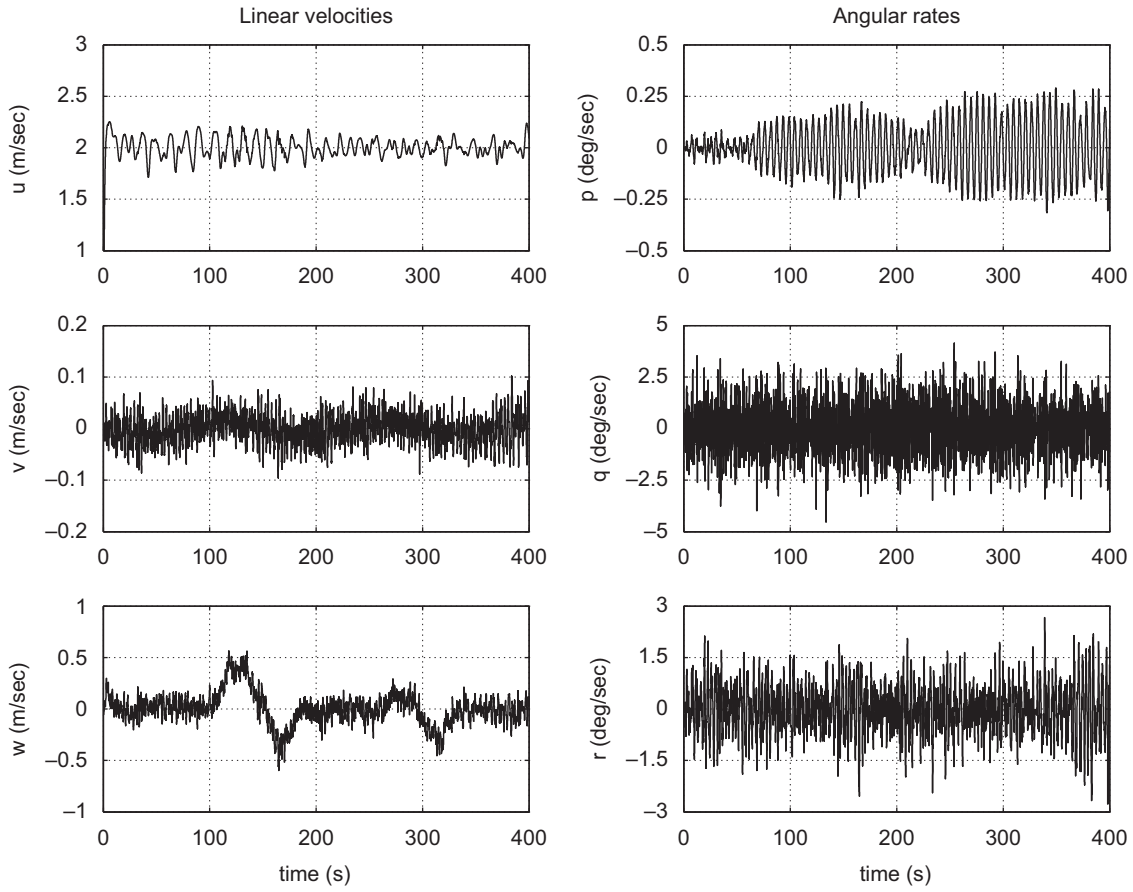

Fig. 18. Linear and angular velocities of the towfish in a bottom-following mission at 4 knts towing speed (Test num. 13).

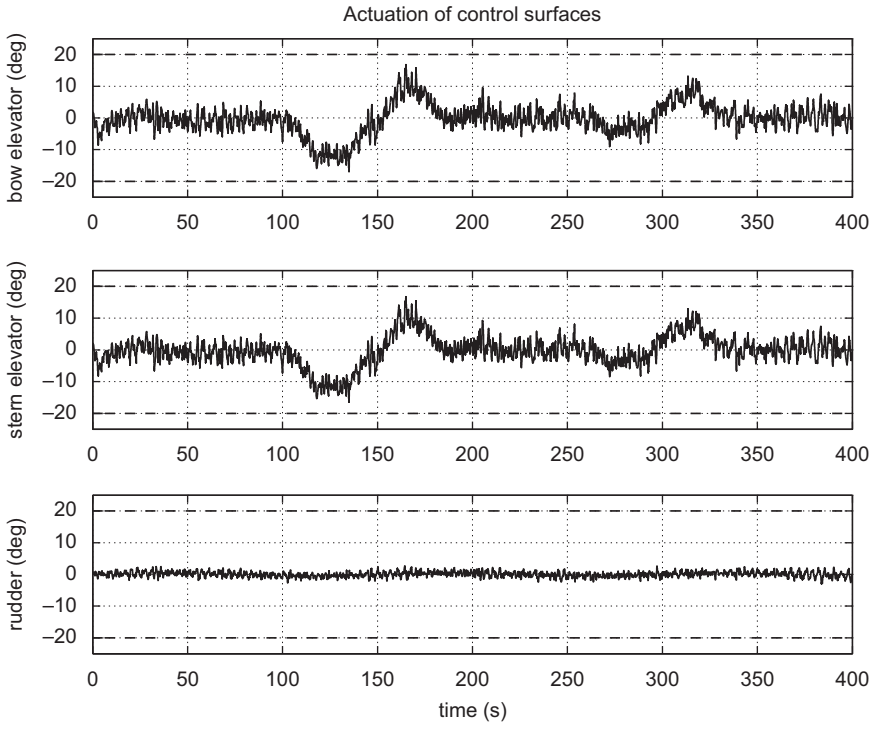

Fig. 19. Actuation of the control surfaces of the towfish in a bottom-following mission at 4 knts towing speed. The upper and lower dashed lines represent the hard-limits of deflection (Test num. 13).

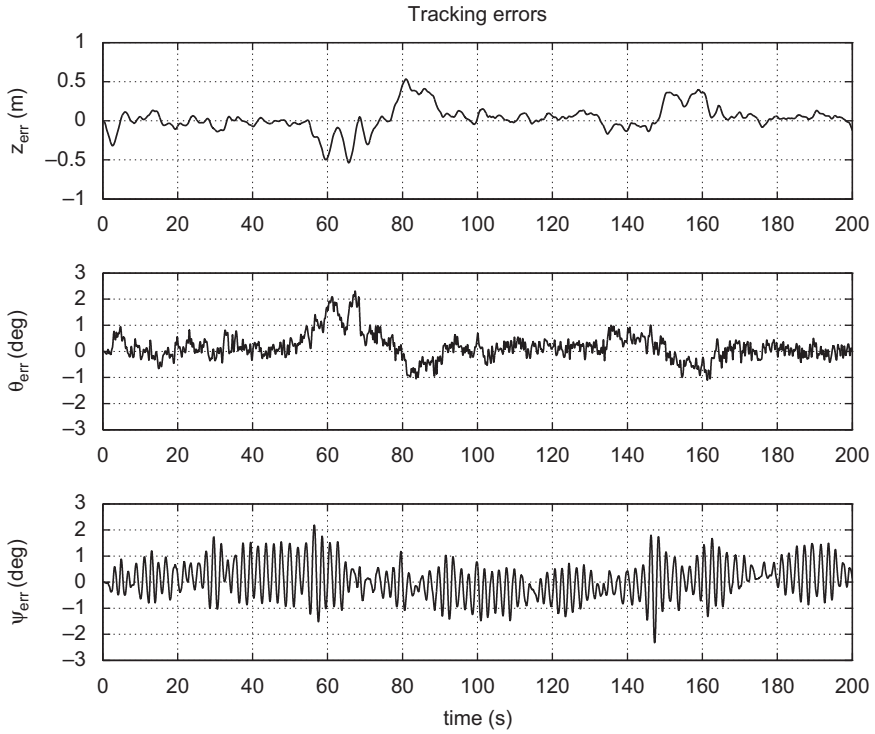

Fig. 20. Tracking errors in a bottom-following mission at 8 knts towing speed (Test num. 14).

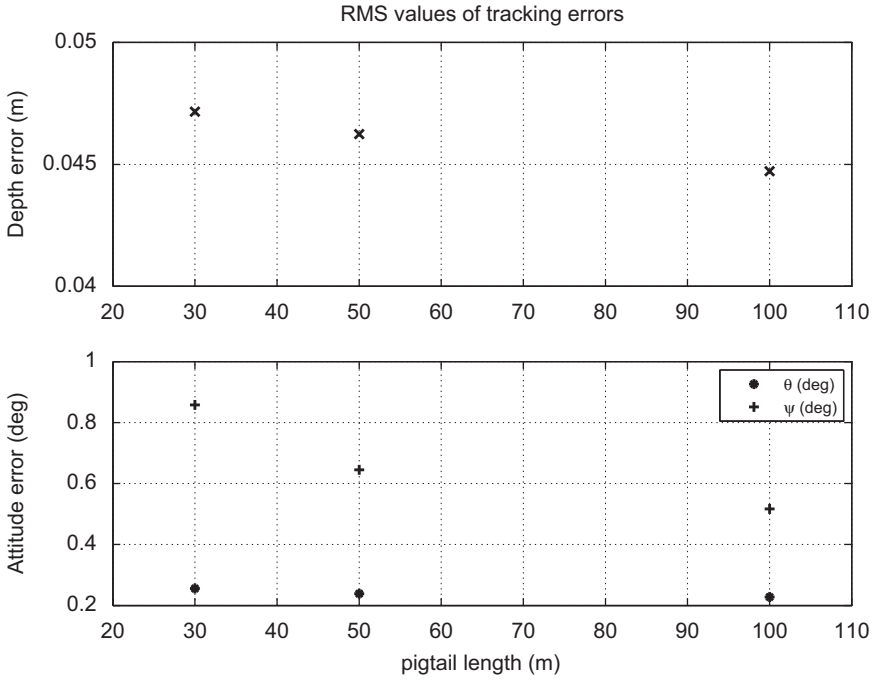

Fig. 21. Impact of different pigtail lengths on system performance. Results obtained with a constant depth trajectory and towing speed of 6 knts (Tests num. 7, 9, and 10).

a long primary cable, a gravitic depressor, and a secondary cable. Although the paper did not address modelling the primary cable, the simulations used realistic wave models to drive the motion of the depressor-pigtail subsystem that transmits the wave driven disturbances to the towfish.

A nonlinear adaptive Lyapunov-based controller was designed and its performance assessed in simulation. Based on the simulation results we concluded that the nonlinear controller proposed is adequate for precise depth control and precise control of the attitude of a towed vehicle. The adaptive controller proved to be robust against vehicle parameter uncertainty and bounded external disturbances. The controlled system exhibits good performance at different equilibrium conditions which are dictated, among other factors, by the length of the secondary

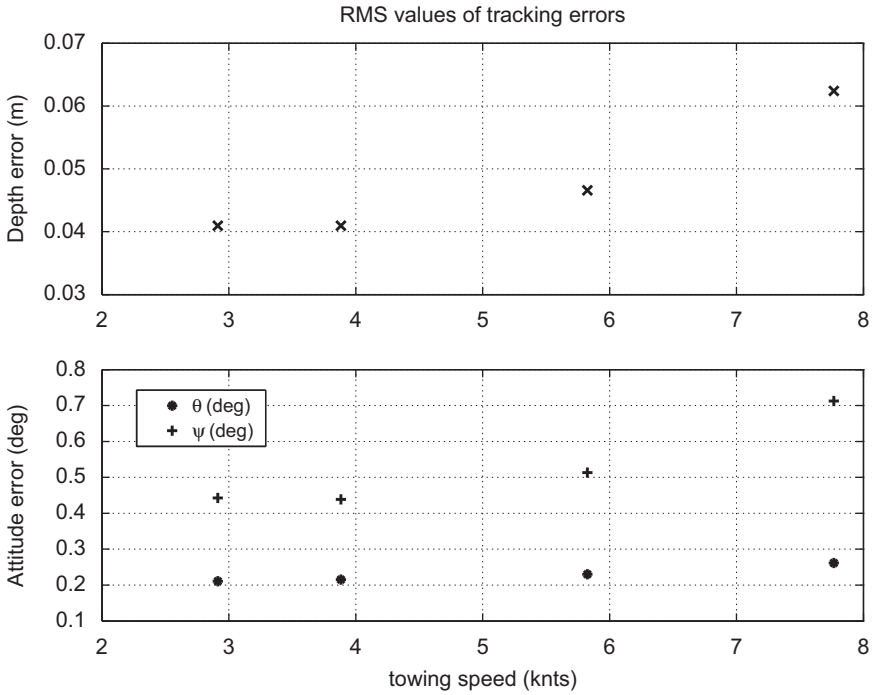

Fig. 22. Impact of different towing speeds on system performance. Results obtained with a constant depth trajectory and a pigtail length of 100 m (Tests num. 5–8).

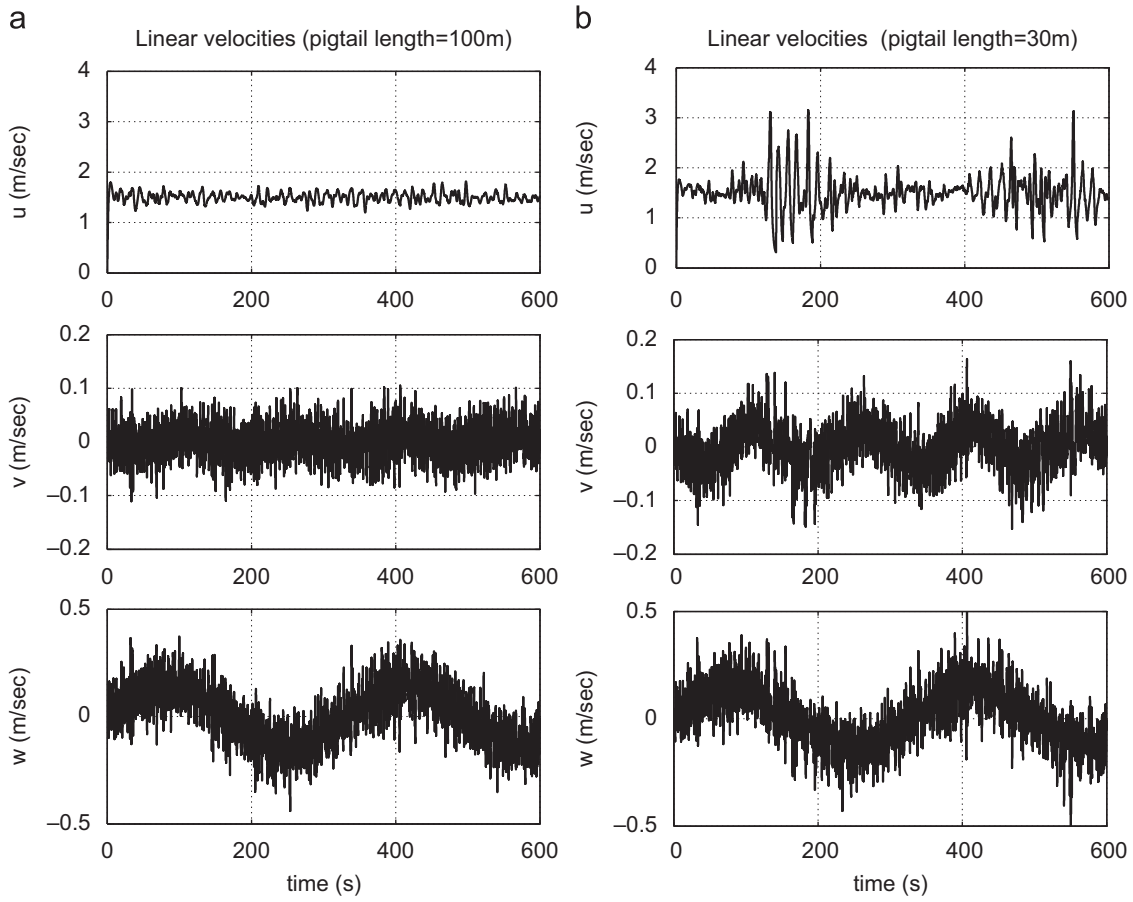

Fig. 23. Impact of different pigtail lengths on linear velocities: (a) pigtail length = 100 m; (b) pigtail length = 30 m (Tests num. 15 and 16, respectively).

cable and the towing speed. The robustness of the adaptive controller was tested in the presence of sensor noise. To simplify practical implementations of the system, no direct measurements are required of surge, sway, and heave speeds. It was shown that the performance of the system is not affected by assuming a constant surge velocity equal to the nominal towing speed.

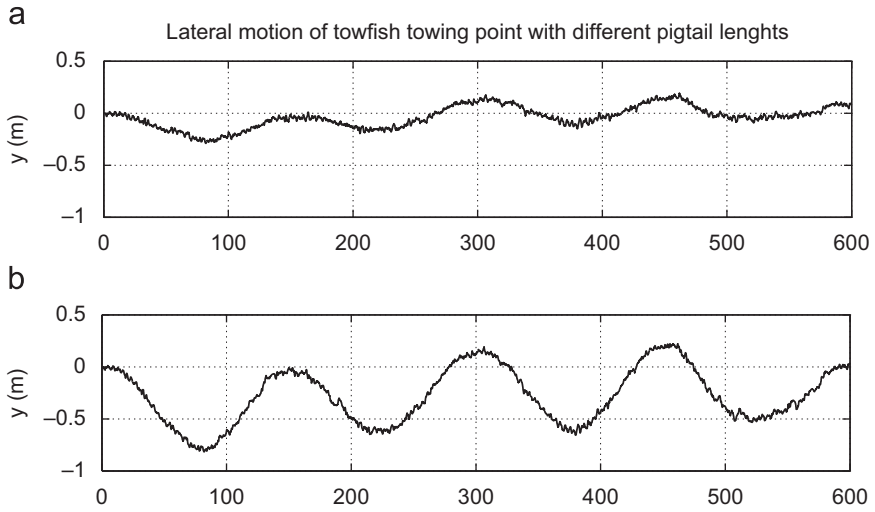

Fig. 24. Impact of different pigtail lengths on lateral motion of the towfish: (a) pigtail length = 100 m; (b) pigtail length = 30 m (Tests num. 15 and 16, respectively).

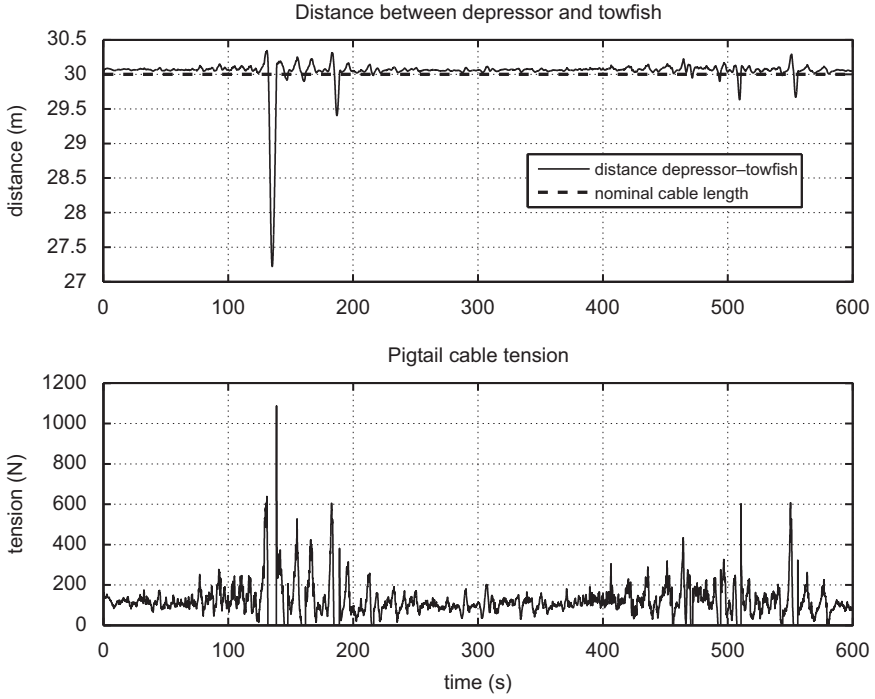

Fig. 25. Distance between depressor and towfish nose and cable tension at 3 knts towing speed (Test num. 16). Notice the impulsive forces that are developed when the secondary cable is suddenly stretched.

A nonlinear observer was derived and proved to be a stable estimator of the heave velocity even in the presence of depth measurement noise.

Although modelling and analysis of the complete towing system was beyond the scope of this work, some concluding remarks on this subject were drawn from the simulations. A pigtail 100 m long is recommended to mitigate accelerations in surge and lateral oscillations of the towfish position. For towing speeds varying from 3 to 8 knts and constant depth tracking, the tracking errors remain inside the specified margin of error. For bottom following missions, unless the proposed specifications can be relaxed, the maximum towing speed recommended is 4 knts.

The results of simulations showed that the tracking errors achieved by the controlled system comply with the specifications imposed by the applications that motivated the system design. With appropriate choices of the pigtail length and towing speed, the magnitude of the depth error is made smaller than 30 cm while pitch and yaw error magnitudes can be made smaller than 1 deg. The absolute value of the roll angle is smaller than 0.25 deg. These conclusions apply to the vehicle model adopted. However, the methodology developed in the paper affords the designer a powerful tool for combined plant-controller design of a large class of towed vehicles.

The paper did not address the problem of control of the lateral position of the towfish. It was shown, however, that in the

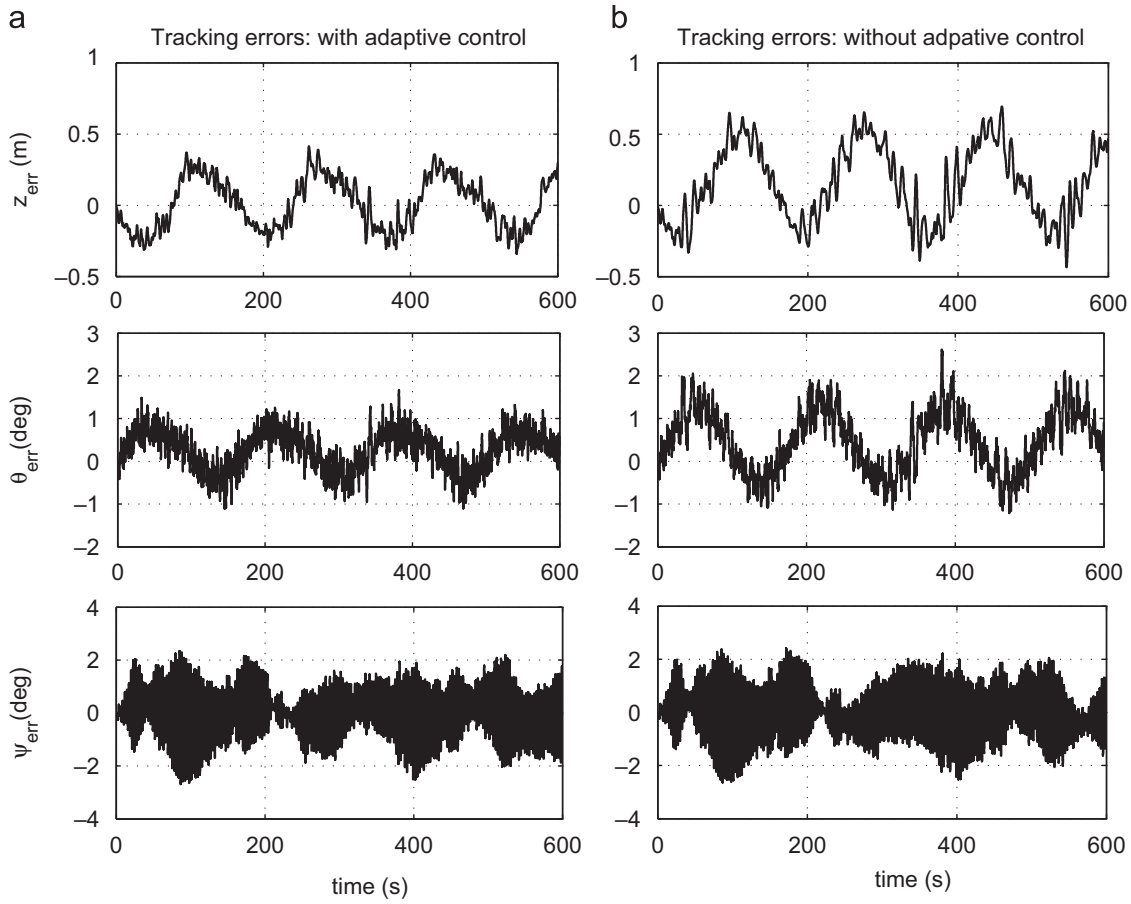

Fig. 26. Impact of adaptive control on system performance; simulation using a sinusoidal trajectory with towing speed 6 knts. (a) With adaptive control; (b) without adaptive control (Tests num. 11 and 12, respectively).

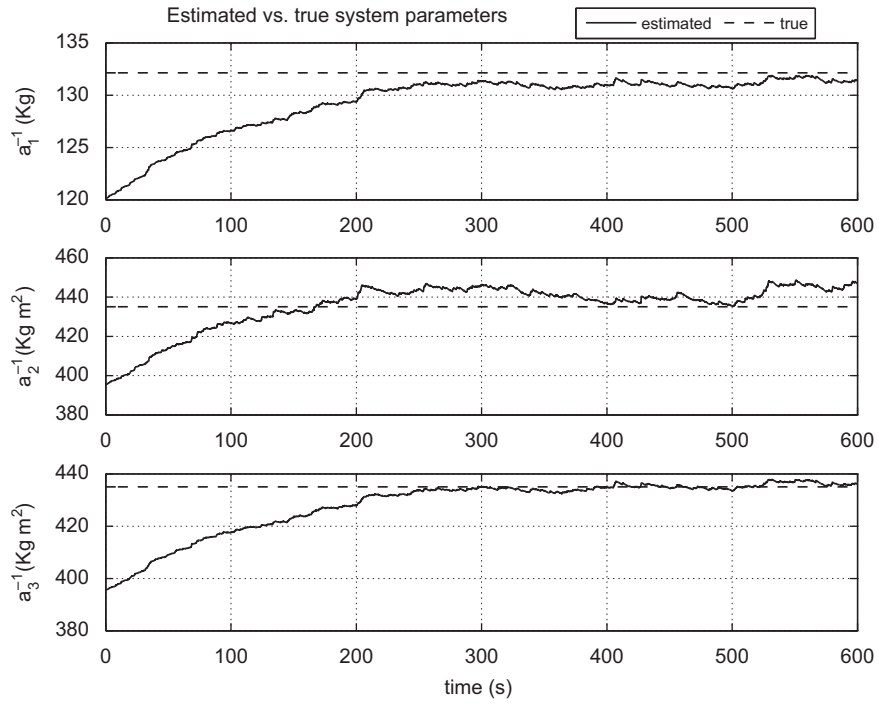

Fig. 27. Parameter estimation implemented in the adaptive controller (Test num. 5).

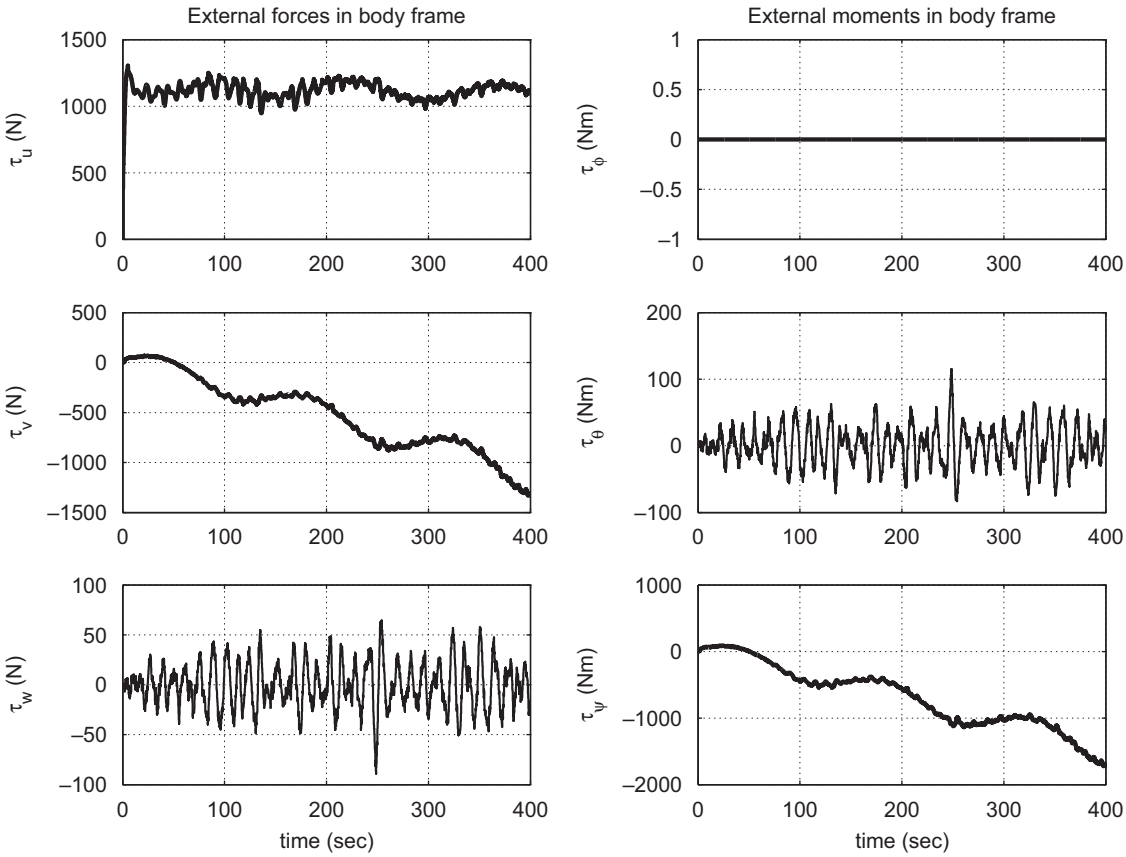

Fig. 28. External forces and moments acting on the towfish at 8 knts towing speed with towfish lateral drift in the presence of 1 knt ocean current; pigtail length of 100 m, constant depth trajectory (Test num. 17).

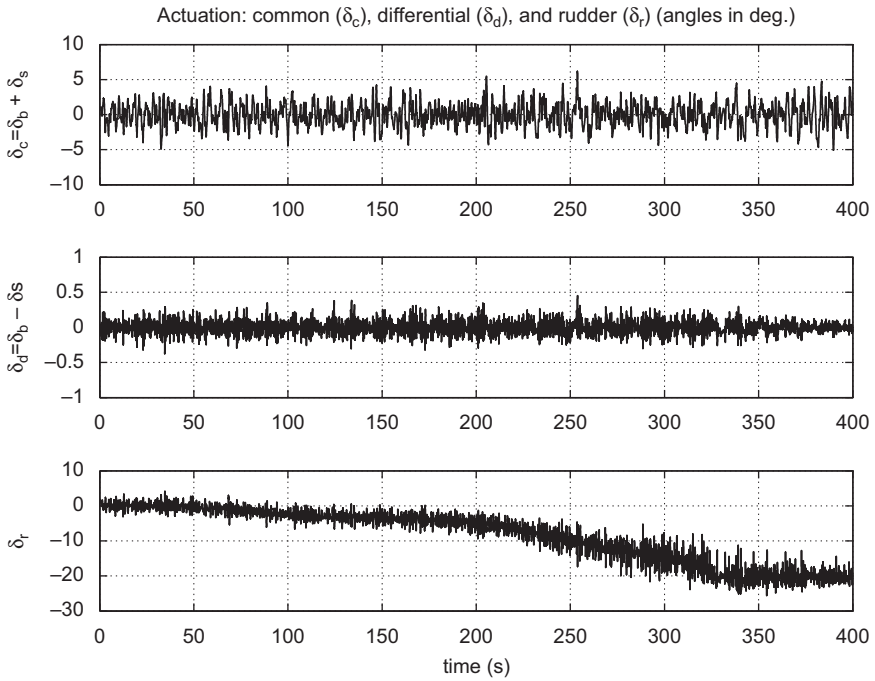

Fig. 29. Actuation of the control surfaces of the towfish with a pigtail of 100 m and 8 knts towing speed in the presence on 1 knt ocean current, constant depth trajectory (Test num. 17).

absence of oceanic currents the lateral motion of the towfish can be kept one order of magnitude smaller than the corresponding displacement of the towing vessel. Even in the presence of underwater currents that cause the vehicle to drift laterally from the desired track, pitch and depth errors are of the same order of magnitude as those observed in the absence of currents. In this scenario, the yaw error becomes slightly biased and orientation control imposes a significantly larger actuation of the rudder. For

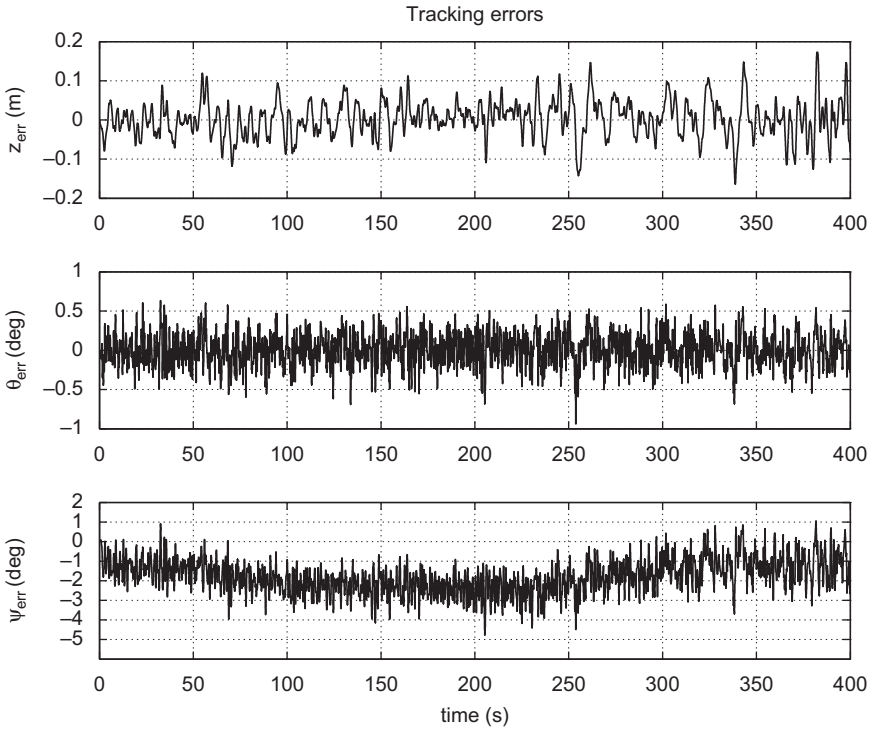

Fig. 30. Tracking errors achieved with a pigtail of 100 m and 8 knts towing speed in the presence on 1 knt ocean current, constant depth trajectory (Test num. 17). Compare these results with those shown in Fig. 11.

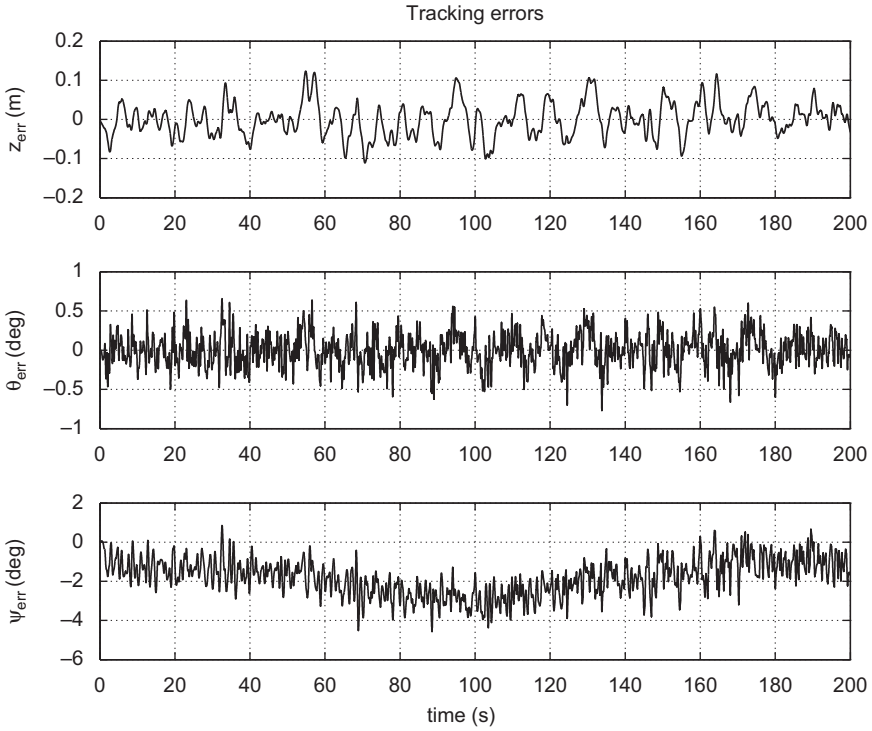

Fig. 31. Tracking errors achieved with a pigtail of 50 m and 8 knts towing speed in the presence on 1 knt ocean current, constant depth trajectory (Test num. 20).

applications that require a precise control of lateral position we propose a fully actuated system equipped with two vertical control surfaces. This will be the subject of future research. We intend to apply in the near future the techniques presented in this study to the control of an actual towfish used in marine geophysical surveying.

Acknowledgements

This research was supported in part by the FREESUBNET RTN of the CEC, projects DENO/FCT-PT (PTDC/EEA-ACR/67020/2006), NAV/FCT-PT (PTDC/EEA-ACR/65996/2006), and EU CO3AUVs, and the FCT-ISR/IST plurianual funding program through the POS C

Program that includes FEDER funds. The work of the first author benefited from a post-doc grant from the Portuguese Foundation for Science and Technology.

Appendix A. Error specifications

The total field magnetic anomaly T_z generated by a dipolar source of dipolar moment M_m at an altitude z from the magnetized body is given by (see e.g. Telford et al., 1998)

$$T_z = \frac{M_m}{z^3}.$$

As a consequence, the error associated to a small variation Δz in the altitude of measurement is

$$T_z - T_{z+\Delta z} = \frac{M_m[(z+\Delta z)^3 - z^3]}{z^3(z+\Delta z)^3},$$

where the units of T, M_m, and z, are respectively, nano-Tesla (nT), Am^2, and m. For a dipolar source, the vertical gradient is given by (see e.g. Breiner, 1973)

$$\left.\frac{\partial T}{\partial z}\right|_z = -\frac{3T}{z},$$

and for small variations of z the error incurred by measuring at altitude $z+\Delta z$ is approximated by

$$\left.\frac{\partial T}{\partial z}\right|_z - \left.\frac{\partial T}{\partial z}\right|_{z+\Delta z} = -\frac{3T}{z}\frac{\Delta z}{(z+\Delta z)}.$$

Consider a typical scenario consisting of a magnetic body located on the sea floor with a dipolar moment $M_m = 10^4\,Am^2$, which generates a magnetic anomaly relative to the Earth's ambient field with amplitude 10 nT at an altitude of 10 m. Elementary computations using the expressions above show that to achieve a maximum error of 1 nT in measurements of the total field anomaly and 0.1 nT/m in gradient measurements at altitude 10 m, the maximum error in the altitude of the magnetic sensors must be approximately 0.3 m.

Appendix B. 6DOF equations of motion

The system inertia matrix structure corresponds to a vehicle with a xz plane of symmetry and is defined as follows:

$$M := M_{RB} + M_A = \begin{bmatrix} \overline{m}-X_{\dot u} & 0 & -X_{\dot w} & 0 & -X_{\dot q} & 0 \\ 0 & \overline{m}-Y_{\dot v} & 0 & -Y_{\dot p} & 0 & -Y_{\dot r} \\ -Z_{\dot u} & 0 & \overline{m}-Z_{\dot w} & 0 & -Z_{\dot q} & 0 \\ 0 & -K_{\dot v} & 0 & I_{xx}-K_{\dot p} & 0 & -I_{xz}-K_{\dot r} \\ -M_{\dot u} & 0 & -M_{\dot w} & 0 & I_{yy}-M_{\dot q} & 0 \\ 0 & -N_{\dot v} & 0 & -I_{xz}-N_{\dot p} & 0 & I_{zz}-N_{\dot r} \end{bmatrix},$$

where M_{RB} is the rigid-body system inertia matrix and M_A is the hydrodynamic system inertia matrix.

The Coriolis and centripetal matrix is

$$C(v) := C_{RB}(v) + C_A(v) = \begin{bmatrix} 0 & -\overline{m}r & \overline{m}q & 0 & -Z_{\dot w}w & Y_{\dot v}v \\ \overline{m}r & 0 & -\overline{m}p & Z_{\dot w}w & 0 & -X_{\dot u}u \\ -\overline{m}q & \overline{m}p & 0 & -Y_{\dot v}v & X_{\dot u}u & 0 \\ 0 & -Z_{\dot w}w & Y_{\dot v}v & 0 & (I_{zz}-N_{\dot r})r - I_{xz}p & -(I_{yy}-M_{\dot q})q \\ Z_{\dot w}w & 0 & -X_{\dot u}u & I_{xz}p - (I_{zz}-N_{\dot r})r & 0 & (I_{xx}-K_{\dot p})p - I_{xz}r \\ -Y_{\dot v}v & X_{\dot u}u & 0 & (I_{yy}-M_{\dot q})q & I_{xz}r - (I_{xx}-K_{\dot p})p & 0 \end{bmatrix},$$

where C_{RB} is the rigid-body Coriolis and centripetal matrix and C_A is the hydrodynamic Coriolis and centripetal inertia matrix.

The transformation matrix from the body-fixed frame $\{B\}$ to the inertial coordinate frame $\{I\}$ is defined as

$$J(\eta) := \begin{bmatrix} J_1 & 0_{3\times3} \\ 0_{3\times3} & J_2 \end{bmatrix}$$

with

$$J_1 := \begin{bmatrix} c\psi c\theta & -s\psi c\phi + c\psi s\theta s\phi & s\psi s\phi + c\psi c\phi s\theta \\ s\psi c\theta & c\psi c\phi + s\phi s\theta s\psi & -c\psi s\phi + s\theta s\psi c\phi \\ -s\theta & c\theta s\phi & c\theta c\phi \end{bmatrix},$$

$$J_2 := \begin{bmatrix} 1 & s\phi t\theta & c\phi t\theta \\ 0 & c\phi & -s\phi \\ 0 & s\phi/c\theta & c\phi/c\theta \end{bmatrix},$$

where $J(\eta)$ also denoted R_B^I is the rotation matrix from the body-fixed frame to the inertial reference frame.

Using the coordinates (x_B, y_B, z_B) of the center of buoyancy of the vehicle, the vector of restoring forces and moments is defined by

$$g(\eta) := \begin{bmatrix} (\overline{W}-\overline{B})s\theta \\ -(\overline{W}-\overline{B})c\theta s\phi \\ -(\overline{W}-\overline{B})c\theta c\phi \\ -z_B\overline{B}c\theta s\phi \\ -z_B\overline{B}s\theta - x_B\overline{B}c\theta c\phi \\ x_B c\theta s\phi \end{bmatrix},$$

where (x_B, y_B, z_B) are the coordinates of the center of buoyancy. The total hydrodynamic damping matrix is

$$D(v) := -\begin{bmatrix} \frac{1}{2}\rho\overline{V}^{2/3}C_x(\alpha,\beta)u & \frac{1}{2}\rho\overline{V}^{2/3}C_x(\alpha,\beta)v & \frac{1}{2}\rho\overline{V}^{2/3}C_x(\alpha,\beta)w & 0 & 0 & 0 \\ \frac{1}{2}\rho\overline{V}^{2/3}C_y(\alpha,\beta)u & \frac{1}{2}\rho\overline{V}^{2/3}C_y(\alpha,\beta)v & \frac{1}{2}\rho\overline{V}^{2/3}C_y(\alpha,\beta)w & 0 & 0 & Y_{|r|r}|r| \\ \frac{1}{2}\rho\overline{V}^{2/3}C_z(\alpha,\beta)u & \frac{1}{2}\rho\overline{V}^{2/3}C_z(\alpha,\beta)v & \frac{1}{2}\rho\overline{V}^{2/3}C_z(\alpha,\beta)w & 0 & Z_{|q|q}|q| & 0 \\ \frac{1}{2}\rho\overline{V}C_K(\alpha,\beta)u & \frac{1}{2}\rho\overline{V}C_K(\alpha,\beta)v & \frac{1}{2}\rho\overline{V}C_K(\alpha,\beta)w & K_{|p|p}|p| & 0 & 0 \\ \frac{1}{2}\rho\overline{V}C_M(\alpha,\beta)u & \frac{1}{2}\rho\overline{V}C_M(\alpha,\beta)v & \frac{1}{2}\rho\overline{V}C_M(\alpha,\beta)w & 0 & M_{|q|q}|q| & 0 \\ \frac{1}{2}\rho\overline{V}C_N(\alpha,\beta)u & \frac{1}{2}\rho\overline{V}C_N(\alpha,\beta)v & \frac{1}{2}\rho\overline{V}C_N(\alpha,\beta)w & 0 & 0 & N_{|r|r}|r| \end{bmatrix}.$$

The forces and moments exerted by the control surfaces are given by

$$\tau := [\overline{u}_u,\overline{u}_v,\overline{u}_w,\overline{u}_K,\overline{u}_\theta,\overline{u}_\psi]^T = \frac{1}{2}\rho\|v_1\|^2 S_s C_{L\alpha}\begin{bmatrix}\frac{(\beta+\delta_r)^2+(\alpha+\delta_b)^2+(\alpha+\delta_s)^2}{\pi\varepsilon_s AR}\\ \beta+\delta_r\\ 2\alpha+\delta_b+\delta_s\\ 0\\ -x_f^1(\delta_b-\delta_s)\\ x_f^1(\beta+\delta_r)\end{bmatrix},$$

where AR is the fin aspect ratio, ε_s is the span efficiency factor, and x_f^i represents the x-coordinate of the hydrodynamic center of the ith fin expressed in the body-fixed frame.

The vector of external forces and moments expressed in the body-fixed referential includes the effects of the towing forces and moments and the external disturbances, as follows:

$$\tau_e := [\tau_u,\tau_v,\tau_w,\tau_\phi,\tau_\theta,\tau_\psi]^T.$$

Appendix C. Model of forces and moments applied to the towfish

The vector $p_d=[x_d,y_d,z_d]'$ that describes the position of the depressor expressed in $\{I\}$ is determined by the model of the depressor motion described in Section 2.6. The model of the forces exerted at the pigtail adapted from Schuch (2004) is as follows.

The spring coefficient of the pigtail is

$$\overline{k}=\frac{E_c}{L_c},$$

where E_c is the elastic modulus of the cable and L_c is the cable length. The distance between the depressor and the tow-point at the fish nose is

$$\Delta L := p_d-\left(\eta_1-R_B^I\begin{bmatrix}L_b/2\\0\\0\end{bmatrix}\right)$$

and the difference between the velocity of the depressor and the tow-point at the fish nose is

$$\Delta v := \dot{p}_d-R_B^I\left(v_1+v_2\times\begin{bmatrix}L_b/2\\0\\0\end{bmatrix}\right).$$

As a consequence, the force applied in the pigtail is

$$f_c := \begin{bmatrix}\overline{k}(|\Delta L|-L_c)+\overline{b}\left(\Delta v'\frac{\Delta L}{|\Delta L|}\right)\\0\\0\end{bmatrix},$$

where $\overline{b}:=2\zeta\sqrt{\overline{k}\overline{m}_u}$ is the damping coefficient, with ζ denoting the damping ratio and $\overline{m}_u:=\overline{m}-X_{\dot{u}}$. Notice that f_c results in a tension force developed in the pigtail *iff* $\overline{k}(|\Delta L|-L_c)+\overline{b}(\Delta v'\Delta L/|\Delta L|)>0$; otherwise the force applied to the towfish is null.

The natural frequency of the pigtail subsystem is given by

$$\omega_n=\sqrt{\frac{\overline{k}}{\overline{m}_u}}.$$

To enter the towfish dynamics, the force f_c is transformed sequentially from the cable coordinate frame $\{C\}$ to frame $\{I\}$ and from this to frame $\{B\}$. The transformation matrix from $\{C\}$ to $\{I\}$ is given by the rotation matrix

$$R_C^I := \begin{bmatrix}c\psi_c c\theta_c & -s\psi_c & c\psi_c s\theta_c\\ s\psi_c c\theta_c & c\psi_c & s\theta_c s\psi_c\\ -s\theta_c & 0 & c\theta_c\end{bmatrix},$$

where the angles $\theta_c:=\sin^{-1}(\Delta z/L_c)$ and $\psi_c:=\sin^{-1}(\Delta y/L_c)$ are illustrated in Fig. 3 with $\Delta z:=z_d-z$ and $\Delta y=:y_d-y$.

Appendix D. Inclusion of coupling terms in system dynamics

D.1. Simplified model with coupling terms

The inclusion of the coupling terms that represent the effects of motion in *roll* in Eqs. (3)–(5) leads to

$$\begin{aligned}&(\overline{m}-Z_{\dot{w}})\dot{w}-Z_{\dot{u}}\dot{u}-Z_{\dot{q}}\dot{q}-(\overline{m}-X_{\dot{u}})uq\\&\quad-Z_{|q|q}|q|q+f_w(v_1,\alpha,\beta)+(\overline{m}-Y_{\dot{v}})vp+g_w(\theta,\phi)\\&\quad=\overline{u}_w(v,\alpha,\delta)+\tau_w,\end{aligned}\tag{41}$$

$$\begin{aligned}&(I_{yy}-M_{\dot{q}})\dot{q}-M_{\dot{u}}\dot{u}-M_{\dot{w}}\dot{w}+(Z_{\dot{w}}-X_{\dot{u}})uw+I_{xz}p^2\\&\quad-(I_{zz}-N_{\dot{r}})rp+(I_{xx}-K_{\dot{p}})rp-I_{xz}r^2-M_{|q|q}|q|q+f_\theta(v_1,\alpha,\beta)+g_\theta(\theta)\\&\quad=\overline{u}_\theta(v,\delta)+\tau_\theta,\end{aligned}\tag{42}$$

$$\begin{aligned}&(I_{zz}-N_{\dot{r}})\dot{r}-N_{\dot{v}}\dot{v}+(X_{\dot{u}}-Y_{\dot{v}})uv-I_{xz}p^2\\&\quad+(I_{yy}-M_{\dot{q}}-I_{xx}+K_{\dot{p}})pq-(I_{xz}-N_{\dot{p}})\dot{p}+I_{xz}rq-N_{|r|r}|r|r+f_\psi(v_1,\alpha,\beta)\\&\quad=\overline{u}_\psi(v,\beta,\delta)+\tau_\psi.\end{aligned}\tag{43}$$

Notice that in Eq. (43) there are two terms than have been neglected in the expressions of the dynamics used by the controller. The term $N_{\dot{p}}\dot{p}$ was eliminated because $N_{\dot{p}}$ is off-diagonal; $I_{xz}\dot{p}$ is neglected because I_{xz} is small and $\dot{p}$ is assumed to be negligible.

D.2. Derivation of Eq. (29)

Eq. (29) is derived as follows:

$$\begin{aligned}\|\Omega_c\|^2&=a_1^2[(\overline{W}-\overline{B})\cos\theta(\cos\phi-1)-(\overline{m}-Y_{\dot{v}})vp]^2\\&\quad+2g_{c1}a_1[(\overline{W}-\overline{B})\cos\theta(\cos\phi-1)-(\overline{m}-Y_{\dot{v}})vp]\\&\quad+2a_2^2[(I_{zz}-I_{xx}+K_{\dot{p}}-N_{\dot{r}})^2p^2r^2+I_{xz}^2p^4-2(I_{zz}-I_{xx}+K_{\dot{p}}-N_{\dot{r}})I_{xz}p^3r]\\&\quad+2a_3^2[(I_{xx}-I_{yy}+M_{\dot{q}}-K_{\dot{p}})^2p^2q^2+I_{xz}^2p^4\\&\quad+2(I_{xx}-I_{yy}+M_{\dot{q}}-K_{\dot{p}})I_{xz}p^3q]\\&\quad+2(g_{c1}^2+g_{c2}^2+g_{c3}^2)\\&\quad\le a_1^2(\overline{m}-Y_{\dot{v}})b_v^2b_p^2+(\overline{W}-\overline{B})^2+2|\overline{m}-Y_{\dot{v}}|b_vb_p|\overline{W}-\overline{B}|\\&\quad+(b_u+b_v)^2+2(b_u+b_v)a_1(|\overline{m}-Y_{\dot{v}}|b_vb_p+|\overline{W}-\overline{B}|)\\&\quad+2[\alpha_1\|X_2\|^2+a_2^2I_{xz}^2b_p^4+\beta_1+\tfrac{1}{2}\|X_2\|^2]\\&\quad+2[\alpha_2\|X_2\|^2+a_3^2I_{xz}^2b_p^4+\beta_2+\tfrac{1}{2}\|X_2\|^2]+2\|X_2\|^2\\&\quad=C_c\|X_2\|^2+\Delta_c,\end{aligned}$$

where $C_c:=2(\alpha_1+\alpha_2+2)$ with

$$\alpha_1:=a_2^2(I_{zz}-I_{xx}+K_{\dot{p}}-N_{\dot{r}})^2b_p^2,$$

$$\beta_1:=2a_2^2(I_{zz}-I_{xx}+K_{\dot{p}}-N_{\dot{r}})^2I_{xz}^2b_p^6,$$

$$\alpha_2:=(I_{xx}-I_{yy}+M_{\dot{q}}-K_{\dot{p}})^2b_p^2,$$

$$\beta_2:=2a_3^2(I_{xx}-I_{yy}+M_{\dot{q}}-K_{\dot{p}})^2I_{xz}^2b_p^6,$$

and Δ_c is a positive constant defined as the sum of remaining terms in the right-hand side of the inequality. In the previous derivation we assumed that the sway velocity and the roll rate are bounded, and applied inequalities of the form $p^2\le b_p^2$ and $vp\le b_vb_p$, where $b_v:=\sup_{t\ge0}|v|$ and $b_p:=\sup_{t\ge0}|p|$. We also used the inequality $g_c=u\tan\theta(1/\cos\theta-1)-v\tan\phi\le K_\theta\ b_u+K_\phi b_v$ which is valid for all $|\theta|,|\phi|\le\pi/2$ with K_θ and K_ϕ real,

non-negative constants. We notice that for small values of θ and ϕ, $g_c \ll b_u + b_v$.

D.3. Derivation of Eq. (32)

From Eqs. (18) and (31) we obtain

$$\dot{V}_3 \le -\lambda V_3 + \frac{C_c}{2\kappa_c}\|X_2\|^2 + \nabla.$$

Since V_3 is a function of X_2, it follows that

$$V_3(t) \le e^{-\lambda t}V_3(0) + e^{-\lambda t}\frac{C_c}{2\kappa_c}\int_0^t \|X_2(\tau)\|^2 e^{-\lambda\tau}\,d\tau + \frac{\nabla}{\lambda}.$$

Defining

$$\gamma_c(X_2) := e^{-\lambda t}\frac{C_c}{2\kappa_c}\int_0^t \|X_2(\tau)\|^2 e^{-\lambda\tau}\,d\tau,$$

the derivative of $\gamma_c(\cdot)$ w.r.t. X_2, for a given $t > 0$ is

$$\frac{\partial\gamma_c}{\partial X_2} = e^{-\lambda t}\frac{C_c}{\kappa_c}\int_0^t X_2(\tau)e^{-\lambda\tau}\,d\tau.$$

Since $\gamma_c(0) = 0$ and $\partial\gamma_c/\partial X_2 > 0$ in the domain $X_2 = [0,\infty)$, by definition $\gamma_c(\cdot)$ is a class K function.

Appendix E. Nonlinear observer of w

It is assumed that the surge and heave velocities verify $u = u_0 \ge 1.5\,\text{m/s}$ and $0 \le w \le 1\,\text{m/s}$, respectively. Under these conditions we can use

$$\tan^{-1}\left(\frac{w}{u}\right)(u^2+w^2) \approx (u_0 + 0.3)w.$$

This approximation improves with increasing u and can be used to simplify the state equation of the observer by linearising the nonlinear terms on w.

E.1. Derivation of Eq. (37)

Take

$$\dot{V}_o = -\tilde{x}_o{}'A_o\tilde{x}_o + 2\tilde{x}_o{}'\tau_o = -\tilde{x}_o{}'A_o\tilde{x}_o + 2\delta_o\tilde{w}(w^2 - \hat{w}^2).$$

Using the equality $w^2 - \hat{w}^2 = \tilde{w}(w+\hat{w})$ we obtain

$$\dot{V}_o = -\tilde{x}_o{}'A_o\tilde{x}_o + 2\delta_o\tilde{w}^2(w+\hat{w}) \le -\tilde{x}_o{}'A_o\tilde{x}_o + 2\|\tilde{x}_0\|^2|\delta_o(b_w+\hat{w})|$$

and therefore

$$\dot{V}_o \le -\tilde{x}_o{}'(A_o - 2|\delta_o(b_w+\hat{w})|I)\tilde{x}_o.$$

To make $(A_o - 2|\delta_o(b_w+\hat{w})|I)$ positive definite the following condition must hold:

$$\begin{bmatrix} 2k_1 - 2|\delta_o(b_w+\hat{w})| & k_2 - \cos\theta \\ k_2 - \cos\theta & -2(C_v + |\delta_o(b_w+\hat{w})|) \end{bmatrix} > 0.$$

This condition is verified if $k_2 \ge 1$, $k_1 > |\delta_o(b_w+\hat{w})|$ and $|C_v| > |\delta_o(b_w+\hat{w})|$ because $C_v < 0$. Given the bound b_w, it is straightforward to show that a sufficient condition for the last inequality to hold is

$$|\tilde{w}| < \frac{|C_v| - \frac{1}{2}\rho S_s C_{L\alpha}\delta_c^{sat} b_w}{\frac{1}{2}\rho S_s C_{L\alpha}\delta_c^{sat}},$$

where $\delta_c^{sat} = \max(|\delta_c|)$ is the hard limit of the common deflection $\delta_c = \delta_b + \delta_s$. Considering the current system's parameters (see Tables 5 and 6), the previous condition establishes the region of attraction of the origin of $\tilde{x}_0$ as

$$|\tilde{w}| < 1.24\,\text{m/s}.$$

Taking in account the bounds on the velocities assumed for the system, this region of attraction is sufficient to ensure convergence of the observer. Notice also that a larger constant C_v improves the convergence of the observer. A larger value of C_v can be achieved by increasing the nominal surge speed u_0 or by increasing the system parameters $C_{L\alpha b}$ or S_s. This is as expected since larger surge speeds and larger $C_{L\alpha b}$ and S_s parameters increase the hydrodynamic efficiency of the control surfaces.

E.2. Stability of the cascade observer-controller system

Given the smooth functions $f_\Omega(\cdot)$ and $f_L(\cdot)$ it is easily observed that (40) is a simplified version of the general interconnected system to which the Generalized Small-Gain Theorem applies; see Jiang et al. (1994). Since the x_2-subsystem is ISpS, then with y_2 as output it has the unboundedness observability (UO) property. The same property applies to the x_1-subsystem. The results of stability analysis in Sections 4.3 and 5.1 are used in the following demonstration. The inequality

$$\begin{aligned}\|\bar{e}\|^2 &\le \frac{1}{2}e^{-\lambda t}[\|\bar{e}(0)\|^2 + \|\bar{z}(0)\|^2 + \frac{1}{m}\|\Pi_0\|_F^2] + \gamma_c(\|X_2\|) + \frac{\nabla}{\lambda} \\ &\le e^{-\lambda t}\|\bar{e}(0)\|^2 + \gamma_c(\|X_2\|) + \frac{\nabla}{\lambda} + \frac{1}{2}\|\bar{z}(0)\|^2 + \frac{1}{2m}\|\Pi_0\|_F^2\end{aligned}$$

follows from (32). From (39) it can be concluded that

$$\tilde{x}_o{}'H\tilde{x}_o \le e^{-\lambda_o t}\tilde{x}_o{}'(0)H\tilde{x}_o(0) + \frac{\Delta_o}{\lambda_o} \le 132.14e^{-\lambda_o t}\|\tilde{x}_o(0)\|^2 + \frac{\Delta_o}{\lambda_o}.$$

Recall the definitions of $x_1 := \bar{e}$, $x_2 := \tilde{x}_o$ and introduce the functions

$$\beta_1(\|x_1(\tau)\|,t) := e^{-\lambda t}\|x_1(\tau)\|^2,$$

$$\beta_2(\|x_2(\tau)\|,t) := e^{-\lambda_o t}\|x_2(\tau)\|^2,$$

$$\gamma_1^u(\cdot) := \gamma_c(\|X_2\|),$$

$$\gamma_1^y(\cdot) := 0,$$

$$d_1 := \frac{\nabla}{\lambda} + \frac{1}{2}\|\bar{z}(0)\|^2 + \frac{1}{2m}\|\Pi_0\|_F^2,$$

$$d_2 := \frac{\Delta_0}{\lambda_0},$$

where β_i are class KL functions, γ_1^u is a function of class K, called the (nonlinear) gain from input to output, and d_i are non-negative constants (for $i = 1,2$). It is immediately verified that

$$\|x_1(t)\| \le \beta_1(\|x_1(0)\|,t) + \gamma_1^u(\|u_1\|) + d_1,$$

$$\|x_2(t)\| \le \beta_2(\|x_2(0)\|,t) + d_2.$$

The remaining conditions of the Generalized Small-Gain Theorem are trivially verified since $\gamma_1^y(\cdot) := 0$. An application of this theorem shows that the cascade system consisting of the observer and the controller is ISpS with respect to bounded disturbances and plant parameter uncertainty as well as bounded noise in the depth measurements used by the observer.

References

Abkowitz, M.A., 1969. Stability and Motion Control of Ocean Vehicles. Massachusetts Institute of Technology.

Blakely, R., 1995. Potential Theory in Gravity and Magnetic Applications. Cambridge University Press.

Breiner, S., 1973. Applications Manual for Portable Magnetometers. Geometrics.

Buckham, B., Nahon, M., Seto, M., Zhao, X., Lambert, C., 2003. Dynamics and control of a towed underwater vehicle system part I: Model development. Ocean Engineering 30 (4), 453–470.

Calkins, D., 1999. A metamodel-based towed system simulation. Ocean Engineering 26 (11), 1183–1247.
Campa, G., Innocenti, M., Wilkie, J., 1996. Model-based robust control for a towed underwater vehicle. In: AIAA Guidance, Navigation and Control Conference, San Diego CA, USA.
Cappell, W.J., Zabounidis, C., Talukdar, K., 1993. Pitch and yaw effects on very wide swath multibeam sonars. OCEANS '93 IEEE Conference, vol. 1. Victoria, Canada, pp. I353–I358.
Chapman, D., 1982. Effects of ship motion on a neutrally stable towed fish. Ocean Engineering 9 (3), 189–220.
Choi, J.-K., Sakai, H., Tanaka, T., 2005. Autonomous towed vehicle for underwater inspection in a port area. In: ICRA 2005—IEEE International Conference on Robotics and Automation, Barcelona, Spain.
Damy, G., Joannides, M., LeGland, F., Prevosto, M., Rakotozafy, R., 1994. Integrated short term navigation of a towed underwater body. In: OCEANS '94 IEEE Conference, vol. 3, Brest, France, pp. 577–582.
Fossen, T.I., 2002. Marine Control Systems. Guidance, Navigation, and Control of Ships, Rigs and Underwater Vehicles. Marine Cybernetics.
Gargett, A.E., 1994. Observing turbulence with a modified acoustic doppler current profiler. Journal of Atmospheric and Ocean Technology 11 (6), 1592–1610.
Hopkin, D., Preston, J.M., Latchman, S., 1993. Effectiveness of a two-part tow for decoupling ship motions. In: OCEANS'93, vol. I, Victoria, Canada, pp. 359–364.
Hubbard, R., 1993. On the towfish motion characteristics of single-body vs. two-body sidescan systems. In: OCEANS'93, vol. 1, Victoria, Canada, pp. I365–I370.
Jiang, Z.P., Teel, A.R., Praly, L., 1994. Small-gain theorem for ISS systems and applications. Mathematics of Control, Signals, and Systems (7), 95–120.
Joannides, M., Le Gland, F., 1993. Position estimation of a towed underwater body. In: 32nd IEEE Conference on Decision and Control, vol.2, S.A. Texas, USA, pp. 1548–1552.
Kato, N., 1987. Vibration analysis of underwater towed system. Journal of the Society of Naval Architects of Japan 162, 363–373.
Kato, N., 1991. Underwater towed vehicle maneuverable in both vertical and horizontal planes. First International Offshore and Polar Engineering Conference, vol. 2. The International Society of Offshore and Polar Engineers, Edimburgh, UK, pp. 85–92.
Kato, N., Koda, S., Takahashi, T., 1986. Motions of underwater towed system. Fifth International Offshore Mechanics and Arctic Engineering Symposium, vol. 3; 1986, pp. 426–433.
Khalil, H.K., 2002. Nonlinear Systems, third ed. Prentice-Hall.
Lambert, C., Nahon, M., Buckham, B., Seto, M., 2003. Dynamics and control of towed underwater vehicle system, part II: model validation and turn maneuver optimization. Ocean Engineering 30 (4), 471–485.
Nasuno, Y., Shimizu, E., Deduka, T., Ito, M., Masuda, M., Aoki, T., 2008. Depth control for towed vehicle. In: OCEANS' 2008—MTS/IEEE Conference, Kobe, Japan, pp. 1–5.
Parker, R.L., 1997. Coherence of signals from magnetometers on parallel paths. Journal of Geophysical Research 102, 5111–5117.
Pascoal, A., Oliveira, P., Silvestre, C., Bjerrum, A., Ishoy, A., Pignon, J.-P., Ayela, G., Petzelt, C., 1997. Marius: an autonomous underwater vehicle for coastal oceanography. IEEE Robotics and Automation Magazine 4 (4), 46–59.
Perrault, D., Hackett, G., Nahon, M., 1997. Simulation and active control of towed undersea vehicles. In: OCEANS '97 MTS/IEEE Conference, vol. 2, Halifax, Canada, pp. 1277–1282.
Preston, J.M., 1989. Stability of towfish as sonar platforms and benefits of the two-part tow. Technical Memorandum 89-19, Research and Development Branch, Department of National Defence, Canada.
Preston, J.M., 1992. Stability of towfish used as sonar platforms. In: OCEANS '92 IEEE Conference, vol. 2, Newport, Rhode Island, USA, pp. 888–893.
Preston, J.M., Poeckert, R., 1993. Distortion and break-up of sidescan images—criteria and reconstruction by geocoding. In: OCEANS '93, vol. 1, Victoria, Canada, pp. I371–I377.
Preston, J.M., Shupe, L., 1993. Remote mine-hunting systems—vehicle stability trials. Technical Report RMC-PROC-93-P-115, Defence Research Establishment Pacific, Victoria, Canada.
Schuch, E.M., 2004. Towfish design, simulation and control. M.Sc. Thesis, Virginia State University, Aerospace Engineering Department.
Schuch, E.M., Linklater, A.C., Lambeth, N.W., Woolsey, C.A., 2005. Design and simulation of a two stage towing system. In: OCEANS 2005 MTS/IEEE Conference, vol. 2, Washington, DC, USA, pp. 1705–1712.
Silvestre, C., Pascoal, A., 1997. Control of an AUV in the vertical and horizontal planes: system design and tests at sea. Transactions of the Institute of Measurement and Control 19 (3), 126–138.
SNAME, 1950. The Society of Naval Architects and Marine Engineers. Nomenclature for treating the motion of a submerged body through a fluid. Technical and Research Bulletin 1 (57).
Spain, P., Fortin, M., 1994. Operational test of a towed ADCP. In: OCEANS'94 IEEE Conference, vol. 1, Brest, France, pp. I424–I428.
Teixeira, F.C., Aguiar, A.P., Pascoal, A., 2006. Nonlinear control of an underwater towed vehicle. In: MCMC'2006—7th IFAC Conference on Manoeuvring and Control of Marine Craft, Lisbon, Portugal.
Telford, W.M., Geldart, L.P., Sheriff, R.E., 1998. Applied Geophysics, second ed. Cambridge University Press.
Tivey, M.A., Johnson, H.P., 2002. Crustal magnetization reveals subsurface structure of Juan de Fuca ridge hydrothermal vent fields. Geological Society of America 30 (11), 979–982.
Tivey, M.A., Johnson, H.P., Bradley, A., Yoerger, D., 1998. Thickness of a submarine lava flow determined from near-bottom magnetic field mapping by autonomous underwater vehicles. Geophysical Research Letters 25 (6), 805–808.
Toda, M., 2005. A theoretic analysis of a control system structure of towed underwater vehicles. In: 44th IEEE Conference on Decision and Control, and the European Control Conference 2005, Seville, Spain, pp. 7526–7533.
Woolsey, C.A., Gargett, A.E., 2002. Passive and active attitude stabilization for a tow-fish. 41st IEEE Conference on Decision and Control, vol. 2. IEEE, Las Vegas, USA, pp. 2099–2104.
Wu, J., Chwang, A.T., 2000. A hydrodynamic model of a two-part underwater towed system. Ocean Engineering 27 (5), 455–472.
Wu, J., Chwang, A.T., 2001a. Experimental investigation on a two-part underwater towed system. Ocean Engineering 28 (6), 735–750.
Wu, J., Chwang, A.T., 2001b. Investigation on a two-part underwater manoeuvrable towed system. Ocean Engineering 28 (8), 1079–1096.
Wu, J., Ye, J., Yang, C., Chen, Y., Tian, H., Xiong, X., 2005. Experimental study on a controllable underwater towed system. Ocean Engineering 32 (14–15), 1803–1817.
Yamaguchi, S., Koterayama, W., Yokobiki, T., 2000. Development of a motion control method for a towed vehicle with a long cable. In: International Symposium on Underwater Technology—UT'00, Tokyo, Japan, pp. 491–496.
Yokobiki, T., 2000. Dynamics and control of a towed vehicle in transient mode. International Journal of Offshore and Polar Engineering 10 (1), 19–25.
Zumberge, M.A., Ridgway, J.R., Hildebrand, J.A., 1997. A towed marine gravity meter for near-bottom surveys. Geophysics 62 (5), 1386–1393.